

Dear Editor,

Enclosed please find the further revised version of **acp-2014-374** paper entitled “**The regime of aerosol asymmetry parameter over Europe, Mediterranean and Middle East based on MODIS satellite data: evaluation against surface AERONET measurements**”. We have addressed the comments by all Reviewers and modified our paper accordingly. More specifically:

- (i) We worked further on section 4, i.e. MODIS-AERONET comparison, re-writing parts of it and removing some others, trying to have it making more sense and being more physically than mathematically based.
- (ii) We provided a more quantitative analysis, especially in sections 4 and 5 (Summary and Conclusions), which hopefully supports the assumptions made for this satellite derived product.
- (iii) We made additional and clear statements on new outcomes from our work and its possible implications for the atmosphere. To this aim, relevant text was added in section 5 (Summary and Conclusions), lines 619 – 644 and 714-734, which hopefully highlights the importance of the present work.
- (iv) We carefully addressed all issues raised and responded to all comments made by the third Reviewer.

I also send you point-by-point responses to the comments of all Reviewers.

Yours sincerely,

Dr Nikos Hatzianastassiou
Laboratory of Meteorology
Physics Department
University of Ioannina
45110 Ioannina
Greece

Tel: ++30 26510 08539
Fax: ++30 26510 08699
email: nhatzian@cc.uoi.gr

Response to Reviewer 1 (Report #2)

We would like to thank the Reviewer for his comments although we were surprised by his verdict. This is because we think that in the previous round of revision we have provided answers to his comments and addressed the raised issues trying to provide necessary clarifications and improvements. Thus we do not understand his statement that “None of my previous remarks were properly addressed”.

Nevertheless, we acknowledge that there might have been some misunderstanding and therefore we tried to further address his requirements from both the first and second rounds of review. More specifically, in this version of the manuscript we re-addressed some of the Reviewer's points from the previous round:

- (i) We added in our manuscript, apart from the definition of asymmetry parameter and discussion of its dependency on aerosol physical and chemical properties (already included at the beginning of sect. 2, lines 102 - 124, from the previous round), a presentation of the retrieval algorithm (method, aerosol modes used), as requested by him. This presentation is given in sect. 2.1, lines 155 - 177.
- (ii) We avoided awkward sentences like “AOD (...) provides a good measure of the aerosol load over an area”.
- (iii) We further explained why we make the study for the selected region and not for the entire globe. We hope that four reasons, given at the end (last paragraph) of the Introduction, lines 78 - 99, are convincing enough on the appropriateness of the study region selection.

Moreover, regarding the statements of the Reviewer on his latest review:

- (i) We believe that the use of Ångström exponent, which satisfied the other Reviewers, significantly supports the findings from the asymmetry parameter analysis, and certainly does not constitute a diversion to the problem of possible uncertainties on MODIS g_{aer} . Given the close relationship between the Ångström exponent and the asymmetry parameter, (both being derived by-products and primarily dependent on aerosol size), we cannot really understand, especially given that no arguments are provided for this, why the use of Angstrom exponent and the presentation of the relevant elaborated results and the associated section (3.2.3) and figures (7 and 8) are not convincing.
- (ii) The paper provides a quantitative assessment of the uncertainties associated with g_{aer} , e.g. related to the calibration issues. To this aim, a whole section (3.2.3, lines 440 - 513) was added dealing with the MODIS g_{aer} uncertainties. However, we acknowledge that probably a satisfactory quantitative reference had not been made on this issue, which is now made in the current revised manuscript (sect. 5, lines 676 – 689 and 714 - 734). We would also like to note that the MODIS g_{aer} uncertainties are further evaluated and quantified through the detailed comparison against the AERONET g_{aer} product (sect. 4, lines 515 - 614). Nevertheless, we acknowledge that probably the previous manuscript

was giving the impression that MODIS g_{aer} data can be used as they are. Therefore, in this modified manuscript we made clear (sect. 5, lines 680 - 683 and 739 - 740) that although g_{aer} data can be used relatively safely, at least to the same degree with Ångström exponent, users should be aware of the g_{aer} uncertainties and their consequences.

Finally, we would just like to kindly note and remind that the Reviewer's reference to the second reviewer comment, that (our paper) "it is a step behind", is not valid any more for the current revised manuscript. Actually, we would like to remind that the specific comment had been made by the other Reviewer on the original manuscript, while he now seems to be satisfied (according to his verdict, i.e. "minor revision") with the revised manuscript.

Response to Reviewer 2 (Report #1)

We would like to thank the Reviewer for his comments. We acknowledge that the AERONET-MODIS comparison section needed to be revised, since it included parts and sentences being focused on numbers and statistics without real physical meaning. Also, its discussion reported sometimes on mathematical findings with not a strong physical interpretation. Accordingly, as suggested by the Reviewer, we worked again on this section and made the following changes so that the manuscript makes more sense and provides the readers with essential and clear information about the MODIS and AERONET g_{aer} data comparison.

- (i) We removed Fig. 11 and its discussion (lines 514-528 in previous revised paper) from the manuscript. This figure was aiming to derive information and conclusions about trends of aerosol asymmetry parameter, using data from both MODIS and AERONET datasets. To this aim, and given the nature of the attempt, severe criteria on data availability were applied in order to ensure robustness of conclusions. Nevertheless, these criteria resulted in a limited number of stations, i.e. 9 stations. But, the worst was that finally, admittedly, the conclusions drawn were not clear at all, i.e. without clear statements on agreement or disagreement or on what MODIS (Terra or Aqua) agrees better with AERONET or on magnitude of trends. Moreover, the conclusions of Fig. 11 were not even substantial, thus consisting and being restricted in reporting numbers. Furthermore, as also noted by Reviewer 3, they were producing some confusion with respect to other similar results, namely those of Fig. 12. We now believe that sect. 4 stands better, being more substantial and to the point. Also note that because of the removal of Fig. 11 and its discussion, Fig. 1 had to be re-made removing the blue squares (9 AERONET stations selected for Fig. 11).
- (ii) In the discussion of Fig. 12, as noted by the Reviewer, there was not possible to draw conclusions on clear spatial patterns regarding the performance of MODIS against AERONET at station level. This has been highlighted in the text, lines 606 - 609, whereas emphasis was given to the degree of correlation between MODIS and AERONET stations data (last paragraph of sect. 4). In order to make more sense with regards to this, the relevant part of the Conclusions section has been re-written, lines 705 - 713.

Response to Reviewer 3 (Report #4)

We would like to thank the Reviewer for his thorough and detailed review as well as for his comments. We have taken care of all of them and modified accordingly the manuscript. Especially, we tried to clarify statements and add references at specific parts of the text, as suggested by the Reviewer. Below are given point by point responses to his comments (also provided in Italics).

- Line 61. References are needed at the end of this sentence.

Done (lines 61-62).

- Line 81. Authors may include some few references out of the Mediterranean basin, focusing on works over subtropical Atlantic, Persian Gulf and Arabian Sea.

References added (lines 81-85).

- Line 86. You may also cite the important article by Ginoux et al. 2012.

Done (line 91).

- Line 101. "namely our study case". This can be deleted.

Done (line 109).

- Lines 198-109. Revise as "'with values increasing with particle size".

Done (line 116).

- Lines 110-113. "The phase ... intensity". A reference is needed here.

Done (line 120).

- Lines 147-150. Authors should clarify that these retrievals correspond to MODIS ocean algorithm.

Done (lines 152 and 155-156).

- Lines 161-162. Revise as “reliable cloud-screened and quality assured Level 2 data.”.

Done (lines 191-192).

- Lines 183-184. Here, a discussion of aerosol hygroscopicity with increase in size and enhancement of scattering processes that lead to higher g is needed with appropriate references.

We would like to note that aerosol hygroscopic growth is a well known issue, as also the dependence of aerosol asymmetry parameter on aerosol size. As suggested by the Reviewer, we have added a short discussion in lines 214-220, stating that: “It should be reminded that the ability of atmospheric aerosol to absorb water affects the particle size (hygroscopic growth), as described by Köhler theory in the early 20th century. It is also well known that relative humidity significantly affects aerosol optical properties (e.g. Pilinis et al., 1996; Kondratyev, 1999), namely AOD, single scattering albedo and g_{aer} , by modifying the aerosol liquid water content, size and hence extinction coefficient and refractive indices. More specifically, aerosol asymmetry parameter increases with increasing aerosol size, as noted in sect. 2.”.

- Lines 191-192. Some references are needed for dust outflows over subtropical Atlantic and Arabian Sea.

Done (line 229).

- Line 224. The reference Gkikas et al. 2014 is missing in the literature list.

Reference was added (lines 809-811).

- Line 232. Correct as “in August”.

Done (line 269).

- Lines 234-235. The reference Prospero et al. (2002) is not so relevant for this sentence. Prospero et al. (2002) used mostly the AI values for the detection of the dust source regions. Especially for Deep Blue retrievals over Middle East and SW Asia, authors may see the Ginoux et al. (2012) paper. Focusing on the annual variability of dust over Middle East and SW Asia, authors may see the papers by Rashki et al. (2012), Rashki et al. (2014).

We would like to thank the Reviewer for his comment, which we agree with. Therefore, we removed the reference Prospero et al. (2002) and cited instead of it (in line 272) the work of Ginoux et al. (2012). We have also made reference to the papers by Rashki et al. (2012, 2014) concerning the annual variability of dust over Middle East and SW Asia (lines 272-274).

- Line 242. A reference is needed for the MODIS Deep Blue AE data.

This sentence refers to the results (not shown in the present study) of our own analysis using MODIS Deep Blue AE data. We have clarified this in lines 280-281.

- Line 248. *“from June to September”*. Shamal wind is also active in spring (March-May). You may see Najafi et al. (2013), Rezazadeh et al. (2013) and references therein.

We agree with this Reviewer’s comment and modified accordingly the text adding relevant references (line 287).

- Line 258. The reference Gkikas et al. 2013 is missing in the literature list.

Reference added in the literature list (lines 805-808).

- Lines 258-261. This annual pattern has to be explained by the seasonal (summer) agricultural biomass burning in Ukraine (see Barnaba et al., 2011; Chubarova et al., 2012).

We thank the Reviewer for this comment. We modified the text (lines 300-303) making reference to the annual cycle of agricultural biomass burning based on existing literature.

- Lines 290-291. Revise as *“Further details and an overall picture is given in the section ...”*.

Done (line 333).

- Line 341. *“...by fine and coarse aerosols”*. Here, you may be more specific by writing that the coarse-mode dust particles have lower spectral dependence of g compared to anthropogenic and biomass-burning aerosols.

Text has been modified accordingly (lines 382-383).

- Line 360. Replace *“changes”* as *“trends”*.

Done (line 400).

- Line 373. Correct as *“than”*.

Done (line 413).

- Lines 430-431. Relative differences as high as 30-40% are detected over large parts of the Atlantic Ocean, which are not in accordance with the discussions here.

We acknowledge that the discussion was incorrect at this point, and we thank the Reviewer for notifying about this. We now modified the text (lines 492-502) so to be in accordance with the figures.

- *Lines 456-457. Which AERONET values did you take for the correlations, the daily-mean or an hourly value close to MODIS overpass? This should be clarified in the manuscript.*

Daily mean AERONET data are used, as specified now in line 524.

- *Line 520-521. This sentence needs revision.*

We would like to note that the whole paragraph (including this sentence), as well as the relevant figure, were removed in this revised manuscript (see our response to Reviewer 2).

- *Figure 7. How you can have correlation between AE and g at northern latitudes where AE values are absent according to Fig. 7a?*

As explained now in the caption of Fig. 7 (and Fig. 8) and in lines 452-454, winter AE data are missing from the northernmost areas and therefore the long-term averages in (a) are left blank. However, the correlation coefficients between $AE_{550-865}$ and g_{aer} data at 660 and 870 nm given in (b) and (c), respectively, are computed from any available data pairs, i.e. available data for both g_{aer} and $AE_{550-865}$ at a given pixel, month and year. This has been clarified in the text (lines 465-470).

- *Figure 8. How can we have values of correlation coefficient, biases and trends at northern latitudes where both Figs 7a and 8a do not contain values?*

Please, see our answer to previous comment. This also answers Reviewer regarding Fig. 8a. A relevant notification was also made in caption of Fig. 8.

References

- Kondratyev, K. Y. 1999. Climatic effects of aerosols and clouds. Springer, New York.
- Pilinis, Ch., Pandis, S. N. and Seinfeld, J. H. 1996. Sensitivity of direct climate forcing by anthropogenic aerosols to aerosol size distribution and composition. *J. Geophys. Res.* 100, 18 739–18 754.

1 **The regime of aerosol asymmetry parameter over**
2 **Europe, Mediterranean and Middle East based on**
3 **MODIS satellite data: evaluation against surface**
4 **AERONET measurements**

5

6 **M. B. Korras-Carraca¹, N. Hatzianastassiou^{2,*}, C. Matsoukas¹, A. Gkikas²,**
7 **C. D. Papadimas²**

8 [1]{Department of Environment, University of the Aegean, 81100 Mytilene, Greece}

9 [2]{Laboratory of Meteorology, Department of Physics, University of Ioannina,
10 45110 Ioannina, Greece}

11

12 Correspondence to: N. Hatzianastassiou (nhatzian@cc.uoi.gr)

13

14 **Abstract**

15 Atmospheric particulates are a significant forcing agent for the radiative energy
16 budget of the Earth-atmosphere system. The particulates' interaction with radiation,
17 which defines their climate effect, is strongly dependent on their optical properties. In
18 the present work, we study one of the most important optical properties of aerosols,
19 the asymmetry parameter (g_{aer}), in the region comprising North Africa, the Arabian
20 peninsula, Europe, and the Mediterranean basin. These areas are of great interest,
21 because of the variety of aerosol types they host, both anthropogenic and natural.
22 Using satellite data from the collection 051 of MODIS (MODerate resolution Imaging
23 Spectroradiometer, Terra and Aqua), we investigate the spatio-temporal
24 characteristics of the asymmetry parameter. We generally find significant spatial
25 variability, with larger values over regions dominated by larger size particles, e.g.
26 outside the Atlantic coasts of north-western Africa, where desert-dust outflow takes
27 place. The g_{aer} values tend to decrease with increasing wavelength, especially over
28 areas dominated by small particulates. The intra-annual variability is found to be
29 small in desert-dust areas, with maximum values during summer, while in all other
30 areas larger values are reported during the cold season and smaller during the warm.
31 Significant intra-annual and inter-annual variability is observed around the Black Sea.
32 However, the inter-annual trends of g_{aer} are found to be generally small.

33 Although satellite data have the advantage of broad geographical coverage, they have
34 to be validated against reliable surface measurements. Therefore, we compare
35 satellite-measured values with g_{aer} values measured at 69 stations of the global surface
36 AERONET (Aerosol Robotic Network), located within our region of interest. This
37 way, we provide some insight on the quality and reliability of MODIS data. We report
38 generally better agreement at the wavelength of 870 nm (correlation coefficient R up
39 to 0.47), while of all wavelengths the results of the comparison were better for spring
40 and summer.

41

42 1 Introduction

43 Atmospheric aerosol particles interact with radiation, mainly the short wave (SW or
44 solar) part of the spectrum, modifying the energy budget of the Earth-atmosphere
45 system. The aerosol effect is either direct, through the scattering and absorption of
46 solar radiation, and thus reducing the incoming solar radiation flux at the surface,
47 indirect, through the modification of cloud properties, or semi-direct, due to the
48 absorption of solar radiation and consequent modification of the atmospheric
49 temperature profile, convection, and cloud properties (e.g. Graßl, 1979; Hansen, 1997;
50 Lohmann and Feichter, 2005).

51 The interaction of particles with the solar flux, which defines their climate role,
52 strongly depends on their optical properties (Hatzianastassiou et al., 2004; 2007),
53 which cannot be covered globally by surface in situ measurements. Besides the
54 aerosol optical depth (AOD), ~~which provides a good measure of the aerosol load over~~
55 ~~an area~~, one of the most important optical properties of atmospheric particles, which is
56 used in radiative transfer, climate, and general circulation models, is the asymmetry
57 parameter (g_{aer}). The asymmetry parameter describes the angular distribution of the
58 scattered radiation and determines whether the particles scatter radiation preferentially
59 to the front or back. The globally available satellite based AOD data are considered to
60 a great extent as reliable and adequate, due to significant developments in surface and
61 satellite measurements during the last two decades, and particularly the arrival of
62 MODIS in 2000, which is regarded as one of the most reliable datasets (Bréon et al.,
63 2011; Nabat et al., 2013)~~after 2000~~. On the other hand, despite ~~of~~ the important role of
64 the asymmetry parameter, relevant global coverage data are measured only for the
65 few last years, or are available in long-term aerosol climatologies such as Global
66 Aerosol Data Set (GADS, Koepke et al. 1997) and Max Planck Aerosol Climatology

67 (MAC, Kinne et al., 2013). Even so, asymmetry parameter data are usually examined
68 for regions with limited geographical extent and temporal coverage (Di Iorio et al,
69 2003), without intercomparison between alternative data platforms.

70 The goal of the present work is the study of the spatiotemporal distribution of the
71 aerosol asymmetry parameter, using the most recent data from MODIS (MODerate
72 resolution Imaging Spectroradiometer, collection 051). Emphasis is given to the
73 comparison between the provided MODIS data and respective reliable surface
74 measurements of the global AERONET, in order to gain insight on the quality of the
75 former.

76 For this study we focus on the region defined by latitudes 5°N to 70°N and longitudes
77 25°W to 60°E, including North Africa, the Arabian peninsula, Europe, and the greater
78 Mediterranean basin (Fig. 1). This area is selected because it is of particular scientific
79 interest due to the simultaneous presence of a variety of particles, both natural and
80 anthropogenic (e.g. desert dust, marine, biomass burning, anthropogenic urban /
81 industrial pollution) as shown in previous studies (Lelieveld et al., 2002; Smirnov et
82 al., 2002; Sciare et al., 2003; Pace et al., 2006; Lyamani et al., 2006; Gerasopoulos et
83 al., 2006; Engelstaedter et al., 2006; Satheesh et al., 2006; Kalivitis et al., 2007; Rahul
84 et al., 2008; Kalapureddy et al., 2009; Alonso-Pérez et al., 2012; Zuluaga et al., 2012;
85 Kischa et al., 2014) which makes this area ideal for aerosol studies. The presence of a
86 variety of aerosols in the area is due to the fact that two of the largest deserts of the
87 planet are partly included in our area of interest, i.e. the Arabian desert and the
88 Sahara, while one finds also significant sources of anthropogenic pollution from urban
89 and industrial centres, mainly in the European continent, ~~with urban and industrial~~
90 ~~centres~~. Moreover, our area of interest and primarily its desert areas, are characterised
91 by a large aerosol load (large optical depth, Remer et al. 2008; Ginoux et al. 2012).
92 Finally In addition, significant regions in this area, more specifically the
93 Mediterranean basin and North Africa, are considered climatically sensitive, since
94 they are threatened by desertification (IPCC, 2007; 2013). Finally, one more reason
95 for the selection of study area is that the present study complements previous ones
96 made by our team (e.g. Papadimas et al., 2008, 2012; Hatzianastassiou et al., 2009)
97 analysing other key aerosol optical properties, namely AOD, for the same region. This
98 is the first study (to our knowledge) that focuses on asymmetry parameter over a
99 geographically extended area, while at the same time compares satellite with ground-
100 station data.

101

102 **2 Data**

103 Before presenting the data used in this study, a short introduction of the parameter
 104 studied is given here for readers more or less unfamiliar with it. The asymmetry
 105 parameter (or factor) is defined by:

106

$$107 \quad g = \frac{\bar{\omega}_1}{3} = \frac{1}{2} \int_{-1}^1 P(\cos\Theta) \cos\Theta d \cos\Theta \quad (1)$$

108 where P is the phase function, which represents the angular distribution of the
 109 scattered energy as a function of the scattering angle Θ and it is defined for molecules,
 110 cloud particles, and aerosols, ~~namely our study case~~. The phase function can be
 111 expressed using the Legendre polynomials $\bar{\omega}_l$ (see Liou, 2002) and $\bar{\omega}_1$ in Eq. (1)
 112 stands for $l=1$. The asymmetry parameter is the first moment of the phase function
 113 and it is an important parameter in radiative transfer. For isotropic scattering, g equals
 114 zero, which is the case for Rayleigh molecular scattering. The asymmetry parameter
 115 increases as the diffraction peak of the phase function sharpens. For Lorenz-Mie type
 116 particles, namely for aerosols and cloud droplets, the asymmetry parameter takes
 117 positive values denoting a relative strength of forward scattering, with ~~increasing~~
 118 values ~~increasing~~ with ~~increasing~~ particle size. It can also take negative values if the
 119 phase function peaks in backward directions (90-180°). The phase function along
 120 with the extinction coefficient (or equivalently the optical depth) and the single
 121 scattering albedo, constitute the fundamental parameters that drive the transfer of
 122 diffuse intensity (Joseph et al., 1976). The asymmetry parameter itself is a simple
 123 expression of the phase function (being its first moment) and it is used in many
 124 radiative transfer and climate models. Hence, the importance of aerosol asymmetry
 125 parameter is easily understood for enabling computations of aerosol radiative
 126 properties and effects (e.g. forcings).

127 Daily data of the aerosol asymmetry parameter (g_{aer}) are used for the needs of this
 128 work. In order to achieve the largest geographical coverage of the studied region, we
 129 employ satellite data from the MODIS-Terra and MODIS-Aqua datasets. These data
 130 are compared with in-situ measurements at stations of the AERONET. We provide a
 131 detailed description of the utilised data in the following sections.

132

133 2.1 Satellite MODIS Terra and Aqua data

134 MODIS is an instrument (radiometer) placed on the polar-orbiting satellites of NASA
 135 (National Aeronautics and Space Administration) Terra and Aqua, 705 km from the
 136 Earth, in the framework of the Earth Observing System (EOS) programme. Terra was
 137 launched on 18 December 1999, while Aqua was launched on 4 May 2002. The two
 138 satellites are moving on opposite directions and their equatorial crossing times are at
 139 10:30 (Terra) and 13:30 (Aqua). MODIS is recording data in 36 spectral channels
 140 between the visible and the thermal infrared (0.44 – 15 μm), while its swath width is
 141 of the order of 2330 km, which results in almost full planetary coverage on a daily
 142 basis. ~~The global MODIS database is generally considered as one of the most reliable~~
 143 ~~at present.~~

144 Aerosol properties are monitored in 7 spectral channels between 0.47 and 2.13 μm
 145 and final results are derived through algorithms developed for aerosol quantities both
 146 over land and ocean (Kaufman et al., 1997; Tanré et al., 1997; Ichoku et al., 2002;
 147 Remer et al., 2005). MODIS data are organised in “collections” and “levels”.
 148 Collections comprise data produced by similar versions of the inversion algorithms,
 149 with the recent collection “051” including also outputs from the “Deep Blue”
 150 algorithm. Levels are characterised by data of different quality analysis and spatial
 151 resolution.

152 In this study we use daily MODIS data for the asymmetry parameter (g_{aer}) provided
 153 on an $1^\circ \times 1^\circ$ grid (namely 100x100 km), from Collection 051, Level 3. These data
 154 were measured at wavelengths 470, 660, and 870 nm, only over oceanic regions, since
 155 they were derived through the algorithm ~~“Dark Target” over ocean for aerosol~~
 156 ~~properties over the ocean~~. The period of analysis stretches from 24-2-2000 to 22-9-
 157 2010 for MODIS-Terra and from 4-7-2002 to 18-9-2010 for MODIS-Aqua.

158 The MODIS C051 g_{aer} data are a derived product of the MODIS algorithm over
 159 ocean. This MODIS algorithm (http://modis.gsfc.nasa.gov/data/atbd/atbd_mod02.pdf,
 160 Remer et al., 2006) retrieves as primary products the AOD at 550 nm, the Fine
 161 (Mode) Weighting (FW, also known as fraction of fine-model aerosol type, FMF) and
 162 the Fine (f) and Coarse (c) modes used in the retrieval, along with the fitting error (ϵ)
 163 of the simulated spectral reflectance. The algorithm reports additional derived
 164 parameters, such as the effective radius (r_e) of the combined size distribution, the
 165 spectral total, fine and coarse AODs or the columnar aerosol mass concentration.
 166 Among them, g_{aer} is also derived and reported at seven (7) wavelengths, 470, 550,

167 660, 860, 1200, 1600 and 2120 nm. The derived parameters are calculated (Levy et
168 al., 2013) from information contained within the look-up table (LUT) and/or other
169 retrieved products. For example, knowing the resulting total AOD and FMF, and
170 which aerosol types were selected (or assumed), one can go back to the LUT, and
171 recover additional information about the retrieved aerosol, such as the g_{aer} . Hence, it
172 should be noted that the derived g_{aer} product is dependent on the used aerosol models
173 (modes), since the algorithm is based on a LUT approach, assuming that one fine and
174 one coarse lognormal aerosol modes can be combined with appropriate weightings to
175 represent the ambient aerosol properties over the target (spectral reflectance from the
176 LUT is compared with MODIS-measured spectral reflectance to find the “best” –
177 least squares – fit, which is the solution to the inversion). In the C051 algorithm there
178 are four fine modes and five coarse modes, for which the spectral (at the afore
179 mentioned 7 wavelengths) aerosol asymmetry parameter values are given in Remer et
180 al (2006).

181 We also used Level 3 daily Ångström exponent data from MODIS-Aqua C051, and
182 also spectral aerosol optical depth data from MODIS-Aqua C006 datasets, from which
183 we computed C006 Ångström exponent. These data were used to assess the validity
184 of g_{aer} data and their temporal tendencieschanges, as discussed in section 3.2.3.

185

186 **2.2 Ground based AERONET data**

187 AERONET (AErosolROboticNETwork) is a global network of stations focused on
188 the study of aerosol properties. AERONET currently encompasses about 970 surface
189 stations (number continuously evolving) equipped with sun photometers of type
190 CIMEL Electronique 318 A (Holben et al., 1998), which take spectral radiation flux
191 measurements.

192 The optical properties of aerosols are extracted through the application of inversion
193 algorithms (Dubovik and King, 2000). Data are provided on three levels (1.0, 1.5, and
194 2). In the present work, we use the most reliable cloud-screened and quality assured
195 Level 2 data, ~~due to their being cloud-screened and quality-assured.~~ AERONET
196 calculates the asymmetry parameter at wavelengths 440, 675, 870, and 1020 nm. We
197 employ daily Level 2 asymmetry parameter data from 69 stations (Fig. 1), contained
198 in our study area (N. Africa, Arabian peninsula, Europe). We choose only coastal
199 stations, in order to maximize the coexistence of satellite marine g_{aer} data with surface

200 data. Also, in order to compare corresponding data between the satellite and station
 201 platforms, we perform comparison only for the 440, 675 and 870 nm.

202

203 **3 Satellite based results**

204 **3.1 Geographical distributions**

205 The spatial distribution of annual mean values of g_{aer} is given in Fig. 2 separately at
 206 the wavelengths 470, 660 and 870 nm. The values are averages over the common
 207 period between Terra and Aqua, namely 4 July 2002 till 18 September 2010. A
 208 significant spatial variability is evident, with MODIS-Terra values varying within the
 209 ranges 0.63 - 0.76, 0.57 – 0.75, and 0.55 – 0.74, at 470, 660 and 870 nm, respectively.

210 The results exhibit a decreasing tendency of g_{aer} with increasing wavelength,
 211 consistent with the theory. Similar results are also obtained from MODIS-Aqua, but
 212 with slightly smaller values than Terra by up to 0.02 on average. More specifically,
 213 the corresponding ranges of wavelengths are 0.63 - 0.75, 0.57 – 0.73, and 0.55 – 0.73.

214 The smaller Aqua than Terra g_{aer} values could be attributed to smaller sizes of
 215 aerosols in midday than morning, corresponding to passages of Aqua and Terra,
 216 respectively, associated with lower relative humidity values and shrinking of aerosol

217 particles. It should be reminded that the ability of atmospheric aerosol to absorb water
 218 affects the particle size (hygroscopic growth), as described by Köhler theory in the
 219 early 20th century. It is also well known that relative humidity significantly affects

220 aerosol optical properties (e.g. Pilinis et al., 1996; Kondratyev, 1999), namely AOD,
 221 single scattering albedo and g_{aer} , by modifying the aerosol liquid water content, size
 222 and hence extinction coefficient and refractive indices. More specifically, aerosol

223 asymmetry parameter increases with increasing aerosol size, as noted in sect. 2. Such
 224 diurnal variation has been also reported for AOD (Smirnov et al., 2002; Pandithurai et

225 al., 2007), but either decreasing or increasing in the day because of the influence of
 226 other factors too, e.g. emissions or wind conditions, apart from aerosol
 227 hygroscopicity.

228 In general, the largest g_{aer} values (deep red colors) are observed off the coasts of West
 229 Africa (eastern tropical Atlantic Ocean) at all three wavelengths. High values are also
 230 found over the Red and Arabian Seas. These high values are due to strong dust
 231 outflows from the Saharan and Arabian deserts carrying out coarse aerosol particles
 232 (Prospero et al., 2002; Alonso-Pérez et al., 2012; Miller et al., 2008) and causing

233 strong forward scattering. Nevertheless, the Persian Gulf region, which is surrounded
234 by deserts, is characterized by relatively smaller g_{aer} values. More specifically, values
235 as small as 0.69 (MODIS-Terra) and 0.67 (MODIS-Aqua) are observed in this region
236 at 470 nm, while at the longer wavelengths (660, 870 nm) the smallest values are
237 equal to 0.66 (Terra) and 0.64 (Aqua). The smaller g_{aer} values over the Persian Gulf
238 can be attributed to the presence of fine aerosols, which is corroborated by the low
239 effective radius and large fine-fraction measurements by MODIS over the Persian
240 Gulf, compared to neighbouring areas (not shown here). These fine particles originate
241 from the industrial activities in the Gulf countries related to oilfields or refineries
242 (Goloub and Arino, 2000; Smirnov et al., 2002a,b; Dubovik et al., 2002).

243 The high g_{aer} values over the northeastern tropical Atlantic Ocean as well as west of
244 the Iberian coasts are possibly related with the presence of coarse sea salt particles.
245 On the other hand, the asymmetry parameter takes clearly smaller values over the
246 Black Sea, where according to MODIS-Terra varies between 0.63 and 0.7 at 470 nm,
247 0.57 and 0.67 at 660 nm, and 0.55 and 0.66 at 870 nm, with the smallest values
248 appearing ~~in~~over the Crimean peninsula (corresponding maximum Aqua values are
249 smaller by 0.02). The small Black Sea g_{aer} values can be associated with ~~the vicinity~~
250 ~~of~~ industrial but also biomass burning activities in nearby countries. A region of
251 special interest is the Mediterranean basin since it hosts a large variety of aerosols like
252 anthropogenic, desert dust or sea salt (e.g. Barnaba and Gobbi, 2004). The MODIS
253 results over this region show relatively small g_{aer} values, secondary to those of Black
254 Sea, characterized by an increase from north to south, which is more evident at 660
255 and 870 nm. More specifically, based on MODIS-Terra, g_{aer} over the Mediterranean
256 takes values from 0.68 to 0.74 at 470 nm, while at 670 and 870 nm it ranges from 0.64
257 to 0.73 and 0.62 to 0.72, respectively. According to MODIS-Aqua the g_{aer} values are
258 slightly smaller again. The observed low values in the northern parts of the
259 Mediterranean are probably associated with the presence of fine anthropogenic
260 aerosols transported from adjacent urban and industrial areas in the north, especially
261 in central Europe. In contrast, the higher g_{aer} values in the southern Mediterranean,
262 particularly near the North African coasts, can be explained by the proximity to the
263 Sahara desert and the frequent transport of significant amounts of coarse dust (e.g.
264 Kalivitis et al., 2006; Hatzianastassiou et al., 2009; Gkikas et al., 2009; 2014).

265 The spatial distributions of climatological monthly mean g_{aer} values from MODIS-
266 Aqua at 470 nm reveal significant differences in the range and the patterns of the

267 seasonal variability, depending on the area (Fig. 3). Thus, in tropical and sub-tropical
 268 areas of Atlantic Ocean (up to about 30°N), where dust is exported from Sahara, g_{aer}
 269 keeps high values throughout the year, which reach or even exceed 0.74 locally. Over
 270 the regions of Arabian and Red Seas and the Gulf of Aden, which also experience
 271 desert dust transport, larger g_{aer} values appear in the period from March to September,
 272 with a maximum ~~on~~in August (locally as high as 0.75-0.76). This seasonal behavior
 273 is in line with intra-annual changes of dust production over the Arabian peninsula
 274 indicated ~~primarily~~ by MODIS ~~Å~~Angström Exponent (AE) and ~~secondarily by~~ Deep
 275 Blue aerosol optical depth data ~~and reported in the literature~~ (Ginoux Prospero et al.,
 276 2002), as well as over southwest Asia through in-situ data (Rashki et al., 2012),
 277 aerosol index from various platforms and MODIS Deep Blue AOD data (Rashki et al.,
 278 2014). Indeed, the production of dust there is relatively poor in winter, increases in
 279 March and April and becomes maximum in June and July (Prospero et al., 2002).
 280 Over the Arabian Sea, it is known that large amounts of desert dust are carried out
 281 during spring and early summer (Prospero et al, 2002; Savoie et al., 1987; Tindale and
 282 Pease, 1999; Satheesh et al., 1999). Nevertheless, according to MODIS, the seasonal
 283 variability of g_{aer} remains relatively small there in line with a small seasonal
 284 variability in MODIS Deep Blue AE data (results of our analysis, not shown here).
 285 This can be explained by the presence of sea salt coarse particles throughout the year,
 286 with which dust particles co-exist.

287 A greater seasonal variability exists over the Persian Gulf, where g_{aer} values are
 288 higher during spring and in particular in summer (up to 0.74 at 470 nm according to
 289 Aqua), and smaller in autumn and winter (area-minimum values smaller than 0.65).
 290 This seasonal behavior can be explained taking into account the meteorological
 291 conditions over the greater area of the Gulf; mainly in spring and summer from June
 292 to September dry northwestern winds (Shamal) blow from northwest carrying desert
 293 dust from the arid areas of Iraq (Heishman 1999; Smirnov et al. 2002a,b; Kutieli and
 294 Furman, 2003). The transport of dust is gradually decreased in autumn and reaches its
 295 minimum in winter~~The transport of dust is gradually decreased in autumn, minimizes~~
 296 ~~in winter and increases again in spring~~. When the presence of desert dust is limited, a
 297 significant fraction of total aerosol load in the region ~~is consisted~~consists of fine
 298 anthropogenic particles (Smirnov et al. 2002a,b), which can explain the observed
 299 relatively small g_{aer} values in autumn and winter.

300 In the Mediterranean basin g_{aer} exhibits a relatively small seasonal variation, ~~though~~
301 ~~with~~ lower values ~~tending~~ to appear in summer and secondarily in early and late
302 spring, in line with the stronger presence of dust in the area, transported from the
303 Sahara desert (Gkikas et al., 2013). On the contrary, over the Black Sea, a clear
304 seasonal cycle is apparent, with higher values in the cold period of the year and
305 smaller in the warm one. More specifically, according to MODIS-Aqua, the values at
306 470 nm drop down to 0.61 in summer months whereas they reach 0.7 in January and
307 December. This seasonality is in agreement with the summer biomass burning from
308 agricultural activities and wildfires (Barnaba et al., 2011; Bovchaliuk et al., 2013),
309 and the resulting abundance of fine particles.

310 It is also interesting to look at the geographical distribution of monthly g_{aer} values in
311 latitudes higher than 50°N, for which annual mean values were not given in Fig. 2
312 because of unavailability of data for all months. Off ~~the coasts of shore~~ northern
313 France (English Channel) and Germany the asymmetry parameter has small
314 seasonally constant values, ~~with a non-significant annual course~~ (note that ~~values data~~
315 do not exist for January and February). In these areas, the aerosol load consists mainly
316 of anthropogenic polluted particles, which explains the small g_{aer} values there.

317 In the Baltic Sea (values available from March to October) g_{aer} shows a significant
318 spatial and temporal variability. More specifically, it is small during summer whereas
319 it increases, locally up to more than 0.7, in March and October. The smaller summer
320 values can be explained by the presence of fine aerosols in the Baltic Sea originating
321 from forest fires in Europe and Russia (Zdun et al., 2011). On the contrary, in autumn
322 the local aerosol loading consists largely of coarse marine aerosols. It is also
323 important to note that the Baltic Sea hosts significant amounts of anthropogenic
324 industrial and urban aerosols throughout the year, but especially in summer (Zdun et
325 al., 2011).

326 In the higher latitudes of Atlantic Ocean, where the presence of maritime aerosols is
327 dominant, ~~it is observed~~ we note a remarkable month by month variation of asymmetry
328 parameter, with low values in summer (values up to 0.59) against high values (up to
329 0.75-0.77) in spring (March, April) and autumn (October). This difference is possibly
330 explained by the seasonal variability of aerosol size in the northern Atlantic. Apart
331 from the presence of coarse sea salt throughout the year, in spring and summer small
332 particles are formed through photochemical reactions of dimethylsulphide (DMS)
333 emitted by phytoplankton decreasing the aerosol size. Moreover during summer fine

334 anthropogenic aerosols are transported in the region from North America (Yu, 2003;
335 Chubarova, 2009). These result in lower g_{aer} values between May and August.

336 Based on MODIS-Terra, the patterns of spatial distribution are generally the same
337 with Aqua, with slightly larger g_{aer} values. At larger wavelengths (660, 870 nm) ~~it is~~
338 ~~observed~~ a decrease of g_{aer} is observed, ~~in particular of especially for~~ its smallest
339 values. Further details and ~~also~~ an overall picture ~~will be~~ given later on, in the
340 section (3.2.1) which deals with climatological monthly mean values not at the pixel
341 but at the regional level.

342

343 **3.2 Temporal variability**

344 **3.2.1 Seasonal variability**

345 In order to provide an easier assessment of the seasonal cycle of aerosol asymmetry
346 parameter and its changes from ~~a one~~ region to another, but also among the different
347 wavelengths (470, 660 and 870 nm), the study region was divided in 6 smaller sub-
348 regions (see Fig. 1). ~~For each sub-region, the~~ The average values of monthly mean
349 climatological data of the pixels found within each sub-region's geographical limits
350 have been computed and are given in Fig. 4, for every wavelength, both and for Terra
351 and Aqua. It appears that the seasonal cycle differs between the sub-regions, as it has
352 been already shown in the geographical map distributions discussed in the previous
353 section.

354 At 470 nm (Fig. 4i), the intra-annual variability of g_{aer} is greater over the Black Sea,
355 where it is as large as 0.06 according to MODIS-Terra and 0.05 according to MODIS-
356 Aqua, the north-eastern Atlantic Ocean (0.04 and 0.05 for Terra and Aqua,
357 respectively) and the seas of North Europe (0.05 for both Terra and Aqua). In these
358 regions, there is a tendency for smaller values during summer. More specifically, in
359 the Black Sea the smallest g_{aer} value (0.64) is observed in June, over the seas of North
360 Europe in July and over the north-eastern Atlantic Ocean in August. In these regions,
361 the largest values appear in the cold period of the year. Reverse seasonality with a
362 large seasonal amplitude is observed over the Persian Gulf, where the variability is as
363 large as 0.08, according to both MODIS-Terra and Aqua. The seasonal cycle of g_{aer}
364 over the Middle East exhibits a smaller range of variability (0.02 for MODIS-Terra
365 and 0.03 for Aqua) along with a reverse seasonal variation, with maximum values in
366 summer and minimum in winter. In the other two sub-regions (Mediterranean and

367 eastern Atlantic Ocean) the annual range of values is small (< 0.02). It is noteworthy
 368 that in the Mediterranean Sea, there is a weak tendency of appearance of double
 369 maxima in winter and spring. The spring maximum should be associated with the
 370 presence of desert dust particles, which are transported from Sahara, mainly in the
 371 eastern Mediterranean in this season (e.g. Fotiadi et al., 2006; Kalivitis et al., 2007;
 372 Papadimas et al. 2008, Gkikas et al. 2009; Hatzianastassiou et al., 2009; Gkikas et al.,
 373 2013). There is also a similar transport of Saharan dust in the central and western
 374 Mediterranean during summer and autumn (e.g. Gkikas et al., 2009; 2013), but then
 375 the predominance is not so clear because of the co-existence of fine anthropogenic
 376 aerosols. Regardless of the annual cycle, smaller g_{aer} values are clearly distinguished
 377 over the Black Sea and North Europe seas throughout the whole year.

378 At 660 nm, the g_{aer} values are lower than at 470 nm, in particular over Black Sea,
 379 North Europe and North-East Atlantic, whereas the intra-annual variability (range of
 380 g_{aer} values) increases up to 0.10 (Terra) and 0.08 (Aqua) over the Black Sea. This
 381 increase is mainly attributed to the reduction of summer values due to the strong
 382 appearance of fine aerosols in this season. Also, at 660 nm, there is a clearer double
 383 annual variation of g_{aer} over the Mediterranean Sea than at 470 nm. At 870 nm the
 384 general picture is similar to that of 660 nm though a further increase of month by
 385 month variability is noticeable.

386 In general, our results indicate that over the regions characterized by a strong presence
 387 of desert dust particles (eastern Atlantic and the Middle East and Mediterranean Seas)
 388 the annual range of variability of g_{aer} is smaller than in the other regions. An
 389 additional feature above regions with desert dust is the smaller decrease of g_{aer} values
 390 with increasing wavelengths, ~~This is which can be~~ attributed to the lower g_{aer}
 391 ~~different spectral dependence of coarse compared to fine particles behavior of solar~~
 392 ~~radiation scattering by fine and coarse aerosols~~ (e.g. Dubovik et al, 2002; J. Bi et al.,
 393 2011).

394 ~~We should note that the It should be noted here that according to our results, using~~
 395 ~~MODIS-Terra and Aqua data, the~~ g_{aer} seasonal cycles ~~is-are~~ about similar but with
 396 generally greater larger Terra than Aqua values.

397 3.2.2 Inter-annual variability and changes

398 Figure 5 displays the geographical distribution of the slope of inter-annual trend of
 399 g_{aer} over the study region, as computed from the application of the Mann-Kendall test

400 to time series of deseasonalized monthly anomalies of g_{aer} at 470 nm. Results are
 401 shown in units decade⁻¹ for both Terra and Aqua over their common time period,
 402 namely 2002 – 2010, only if the trend is statistically significant at the 95% confidence
 403 level. We also performed the same analysis for the 660 and 870 nm (not shown), with
 404 similar results to the 470 nm wavelength.

405 In general, the estimated changes are relatively small. Terra produces widely
 406 statistically significant positive trends, showing that during the period of interest, the
 407 asymmetry parameter increased over the examined area, with very few exceptions.
 408 The results from Aqua are statistically significant at considerably fewer cells, but also
 409 give a few points with decreasing g_{aer} . Based on Terra data, the stronger increases are
 410 observed in the eastern and southern Black Sea, as well as over the Baltic and Barents
 411 Seas. According to MODIS-Aqua, negative ~~changes-trends~~ are found over few
 412 Atlantic Ocean cells. Both Aqua and Terra report increases of g_{aer} over the Persian
 413 Gulf, the Red Sea, South Black Sea, East Mediterranean, the coast of the Iberian
 414 Peninsula, and some coastal areas of West Africa. The differences encountered
 415 between the Terra and Aqua g_{aer} trends may be attributed to the different time of
 416 passage of each satellite platform carrying the same MODIS instrument, given that
 417 everything else is the same. Nevertheless, ~~most probably,~~ they may more probably be
 418 the result of calibration differences between the two MODIS sensors. It is known that
 419 there is a degradation of MODIS sensor (Levy et al., 2010; Lyapustin et al., 2014)
 420 impacting time series of MODIS products. More specifically, it is also known that
 421 Terra suffers more than Aqua from optical sensor degradation. These calibration
 422 issues are known to affect MODIS AOD retrievals, producing an offset between Terra
 423 and Aqua, and they are also expected to affect aerosol asymmetry parameter, which is
 424 probably more sensitive to such calibration uncertainties ~~that than~~ AOD. In this sense,
 425 the results of Fig. 5 shown here are not to be taken as truth but rather they are given as
 426 a diagnostic of a problematic situation with MODIS aerosol asymmetry parameter
 427 inter-annual changes. Such calibration issues are expected to be addressed, at least
 428 partly, in the new Collection 006 products. Nevertheless, a preliminary comparison
 429 between MODIS Aqua ~~C051C005~~ and C006 ~~Å~~Angström exponent (AE), which is
 430 another common aerosol ~~size~~-parameter strongly dependent on size, using ~~AE~~-data for
 431 the 550-865 pair of wavelengths spanning the period 2002-2010, does not reveal
 432 significant modifications in geographical patterns of AE inter-annual changes. This
 433 puts some confidence on the C051 g_{aer} results given in the present study. The results
 434 of this analysis are presented in detail in the next sub-section (3.2.3).

435 The overall g_{aer} changes of Fig. 5 may hide smaller timescale variations of g_{aer} , which
 436 are obtained by the time-series shown in Fig. 6. Results are given for the 7 sub-
 437 regions defined previously, at the three different wavelengths and for Terra and Aqua
 438 separately. A general pattern is the decrease of g_{aer} values with increasing wavelength,
 439 in particular from 470 to 660 nm. The largest month to month and year to year
 440 variation is for Black Sea (Fig. 6i). Relatively large variability is also found in the
 441 sub-regions of NE Atlantic (6v), North Europe (6vi) and the Persian Gulf (6vii). On
 442 the contrary, small variability is noticed in the eastern Atlantic, where systematic dust
 443 outflows from Sahara take place leading to consistently high values of g_{aer} . There are
 444 also some other interesting patterns, like the significant drop of g_{aer} with wavelength
 445 in areas characterized by the presence of fine aerosols, namely the Black Sea, North
 446 Europe and the Persian Gulf (Figs. 6i,vi,vii, respectively). The specific patterns of
 447 inter-annual changes of g_{aer} are suggested by both Terra and Aqua, though a slight
 448 overestimation by Terra is again apparent in this figure. The obtained results of our
 449 analysis are meaningful and in accordance with the theory, underlining the ability of
 450 satellite observations to reasonably capture the g_{aer} regime over the studied regions.

451 3.2.3 Possible uncertainties of MODIS aerosol asymmetry parameter

452 The MODIS aerosol asymmetry parameter is not a direct retrieval product of the
 453 MODIS retrieval algorithm, but it is rather a derived ~~by-product~~ ~~by product~~. Since this
 454 parameter is dependent on aerosol modes used and relative weights, it is understood
 455 that there can be uncertainties associated with it. Therefore questions may arise about
 456 the validity of g_{aer} and their spatial and temporal patterns presented in the previous
 457 sub-sections. Given that, as ~~it was~~ already mentioned, it is an aerosol optical
 458 parameter that is valuable and highly required by radiative transfer and climate
 459 models, it is worth assessing it through comparison against another more common
 460 aerosol size parameter, namely the ~~C051C005~~ MODIS Ångström exponent at the
 461 550-865 nm wavelength pair ($AE_{550-865}$) over ocean, which is an evaluated MODIS
 462 aerosol size product (Levy et al., 2010) that is extensively used in literature. Figure
 463 7a, displays the geographical distribution of long-term average AE for the whole
 464 study period, i.e. 2002-2010. In this figure, the northernmost areas are blank with
 465 respect to g_{aer} (Fig. 7a) because there are no data during winter and a long-term
 466 average would be biased. The main geographical patterns in Fig.7a are in line with
 467 those of asymmetry parameter (Fig. 2). For example, note the high AE values in the
 468 Black Sea (between about 1.3 and 1.8, yellowish-reddish colors), indicative of fine

469 aerosols, the relatively high values in the Mediterranean Sea (between about 0.7 and
 470 1.2, greenish-yellowish colors) and the low values (0.1-0.4, deep bluish colors) off the
 471 western African coasts corresponding to exported Saharan dust. Over the same areas,
 472 g_{aer} takes inverse low and high values, for example smaller than 0.65 over the Black
 473 Sea and larger than 0.7-0.75 off the western African coasts (Figs 2ii-b and 2iii-b),
 474 indicating the predominance of fine and coarse aerosols respectively, in accordance
 475 with AE. The consistency between g_{aer} and AE data is shown by the strong anti-
 476 correlation between the MODIS $AE_{550-865}$ and g_{aer} data at 660 and 870 nm, shown in
 477 Figures 7b and 7c, respectively. It should be noted that correlation coefficients are
 478 computed from any available data pairs, i.e. available data for both g_{aer} and $AE_{550-865}$
 479 at a given pixel and day. Note that there are no blank areas in Figs 7b and 7c, opposite
 480 to Fig. 7a, because as there are both AE and g_{aer} data for all but winter months,
 481 correlation coefficients can be calculated for these regions (Figs. 7b, 7c). Strong
 482 negative correlation coefficients, larger than 0.7 and 0.8 in Figs 7b and 7c,
 483 respectively, relate inversely high/low g_{aer} values with low/high AE ones and vice-
 484 versa, over the same areas. In both cases (Figs 7b and 7c), the correlation is slightly
 485 higher over sea areas characterized by the presence of fine aerosols (e.g. Black Sea or
 486 Persian Gulf) and lower over seas undergoing frequent transport of coarse dust
 487 particles (e.g. southern Mediterranean Sea, Arabian Sea or Atlantic Ocean off the
 488 western African coasts). The overall computed correlation coefficient between g_{aer} and
 489 AE is equal to -0.95 over the Black Sea, -0.89 over the Mediterranean Sea, -0.87 and -
 490 0.94 over the Arabian Sea and Persian Gulf, respectively and -0.89 off the western
 491 African coasts (values given for $AE_{550-865}$ and g_{aer} data at 870 nm). These results
 492 indicate that the spatial patterns of MODIS $C051C005$ g_{aer} product are reasonable as
 493 compared to the $C051C005$ Ångström exponent data. This shows that the use of g_{aer}
 494 in modeling studies can be considered as reasonably reliable with regards to the
 495 consideration of fine and coarse aerosols over the examined study area, with slightly
 496 more confidence over areas characterized by the presence of fine particles, such as the
 497 Black Sea or Persian Gulf.

498 Since questions may also arise about possible uncertainties regarding the long-term
 499 variability of MODIS $C051C005$ aerosol size products, due to the calibration issues
 500 discussed in the previous section, the corresponding MODIS C006 AE product is
 501 displayed in Fig. 8a. ~~From Figs. 8a and 7a a-are similarity is apparent~~ in the main
 502 geographical patterns of the two collections' AE product. The similarity between
 503 $C051C005$ and C006 AE data is also depicted in the computed correlation coefficients

(Fig. 8b), exceeding 0.8, and biases (in absolute and relative percentage terms, Figs 8c and 8d, respectively). For the Mediterranean Sea, the Arabian Sea and Persian Gulf, biases which are smaller than 0.1 or 10% in most areas ~~of the study region~~ and 0.2 or 20% almost everywhere. Relative biases larger than 30% are only observed over the open Atlantic Ocean. The overall computed correlation coefficient for the entire study region is 0.88 (0.86, 0.89, 0.95 and 0.84 for Mediterranean, Arabian, Persian and Atlantic sea surfaces off the western African coasts). The corresponding overall relative percent bias is equal to 15.6% (9.1, 6.7, 6.1 and 15.7 for the same sub-areas as above). Our results indicate that the uncertainty related to the use of C051 AE data is small, especially over the Mediterranean Sea, the Arabian Sea, the Persian Gulf and the Atlantic Ocean areas not far from the European, African and Asian coastlines. ~~It should be noticed that~~ Our AE results are in line with those of Levy et al. (2013, Fig. 15) which refer, however, only to year 2008 (ours are for 2002-2010). In addition, a comparison is attempted in Figs 8e and 8f between the computed trends of C051 and C006 AE data over the common period 2002-2010, in order to assess whether changes are detected, which could be an indication of possible changes in corresponding asymmetry parameter trends. Figures 8e and 8f show the computed deseasonalized trends of slope values for both ~~C051~~ and C006 AE. The results reveal similar patterns between ~~C051~~ and C006. Small trends are found in both of them, in agreement with the small trends of asymmetry parameter reported in Fig. 5. We find ~~it is found~~ that the sign of AE trends basically~~mainly~~ does not change from C051 to C006. This might be a signal that no changes of aerosol asymmetry parameter are expected in C006 and puts ~~some~~ confidence on the C051 results given in the present study.

528

529 **4 Evaluation against AERONET data**

530 In this section we compare the satellite-measured aerosol asymmetry parameter with
 531 measurements from the global network of surface stations of AERONET, which is
 532 considered as the reference dataset (Holben et al., 1998). For this purpose, we
 533 identified the AERONET stations inside our area of interest and finally utilised only
 534 the coastal ones, so that both satellite and surface data be available. The total number
 535 of these stations is 69, and their locations are shown in Fig. 1 (open and full circles)
 536 (blue squares).

537 Table 1 contains the comparison statistical metrics for all wavelengths (Pearson
 538 correlation coefficient, bias, root mean square error (RMSE)~~standard deviation~~, slope,
 539 intercept) of the comparison between surface daily mean data from AERONET and
 540 satellite data from MODIS-Terra and MODIS-Aqua, which correspond to the $1^\circ \times 1^\circ$
 541 cell wherein each station is located. For this analysis, we use all cells and days with
 542 common data between Terra-AERONET and Aqua-AERONET. The mean
 543 differences are calculated as $g_{\text{aer}}(\text{AERONET}) - g_{\text{aer}}(\text{Aqua})$ and $g_{\text{aer}}(\text{AERONET}) -$
 544 $g_{\text{aer}}(\text{Terra})$.

545 In general, we may note that on an annual level, the MODIS-Terra and Aqua
 546 asymmetry parameter values at 470 nm are not in very good agreement with the
 547 respective data from AERONET at 440 nm, while the results at the largest
 548 wavelengths are more reassuring, though not being very satisfactory (increasing R and
 549 decreasing relative bias and RMSE values at 675/660 nm and 870 nm). At 870 nm
 550 (Table 1 and Fig. 9), correlation coefficients are found to be the largest and equal to
 551 0.47 (AERONET-Terra) and 0.46 (AERONET-Aqua), while satellite data are slightly
 552 overestimated compared to the surface data (bias -0.035 or 5.54% and -0.015 or -
 553 2.43%, respectively).

554 It is important to note that the agreement of satellite and surface data is better in
 555 spring and summer, for all studied wavelengths. Specifically, in case of MODIS-Aqua
 556 g_{aer} , the correlation coefficients increase up to 0.35, 0.50 and 0.54 at 440/470 nm,
 557 660/675 nm and 870 nm, respectively, while the bias decreases down to 0.0005
 558 (0.07%), 0.003 (0.46%) and 0.007 (1.11%), respectively.

559 Moreover, we find that for all seasons g_{aer} values at 870 nm and 660 nm, both from
 560 MODIS-Terra and MODIS-Aqua, are overestimated compared to $g_{\text{aer}}(\text{AERONET})$ at the
 561 corresponding wavelengths (stronger overestimation at 870 nm and by Terra). Finally
 562 we note an underestimation of g_{aer} at 470 nm from MODIS-Aqua, relative to the data
 563 by AERONET at 440 nm, while very small biases (<0.5 %) are found between Terra
 564 and AERONET at the same wavelengths.

565 In Fig. 9 we present a scatterplot comparison between MODIS and AERONET g_{aer}
 566 data pairs. There is bias towards larger g_{aer} values from both Aqua and Terra
 567 compared to AERONET, with Terra overpredicting more than Aqua. The root mean
 568 square error to the fit between MODIS and AERONET is very similar between Aqua
 569 and Terra. There are concerns on the application of ordinary least squares regression,
 570 arising from the assumption that as the assigned independent variable, AERONET
 571 values should be free from error. We cannot guarantee the validity of this assumption,

572 so we recognize that the reported R and slope values from Fig. 9 and Table 1, if
573 viewed as metrics of agreement between MODIS g_{aer} and real g , may be subject to the
574 effect of regression dilution and consequently biased low. This possible bias for R and
575 slope could be neglected only if AERONET errors can also be considered negligible.
576 With the above caveat in mind, the applied least-squares fit line to the scatterplot
577 comparison between matched MODIS-AERONET data pairs (Fig. 9) indicates that
578 MODIS overestimates g_{aer} more in the smaller than larger values, i.e. more for fine
579 than coarse particles.

580 We present the frequency distributions of asymmetry parameter daily values (Fig. 10)
581 on the days when data from all three databases (MODIS-Terra, MODIS-Aqua and
582 AERONET) were provided. Fig. 10a corresponds to the whole area of interest, while
583 Figs. 10b and c correspond to two broad sub-regions with basic differences in the
584 aerosol source, namely Europe with great anthropogenic sources, and Africa, Middle
585 East and Arabian peninsula, with predominant natural sources and mainly desert dust.
586 There is an apparent skew in the MODIS-Terra and MODIS-Aqua g_{aer} distributions,
587 while the AERONET distributions are more symmetrical. Moreover, the satellite data
588 distributions show larger values and smaller standard deviations compared to
589 AERONET, with the Terra overestimation being more exaggerated. The disagreement
590 is more pronounced in the sub-region of Europe, while in the sub-region of North
591 Africa / Arabian peninsula, the distributions of satellite and surface data agree more
592 thus confirming the finding of Fig. 9 based on the slope of applied linear regression
593 fit. Values over Europe are generally smaller than over North Africa / Arabian
594 peninsula (Fig. 3), which can be attributed to the presence of larger size particles of
595 desert origin in the latter sub-region, in contrast to Europe, where due to industrial
596 activity and frequent biomass burning the presence of smaller size particles is
597 important. Therefore, the smaller g_{aer} values (<0.6) in the frequency distributions of
598 the whole area, are overwhelmingly contributed by the European sub-region,
599 contrasting with larger values (0.7-0.75) being contributed by both sub-regions and
600 even more by N. Africa/Arabian peninsula at larger g_{aer} .

601 ~~Potentially useful results may be derived by the comparison of the temporal trends~~
602 ~~from satellite and surface data. We show in Fig. 11 the absolute and relative changes~~
603 ~~of the asymmetry factor, calculated through regression on monthly time series of g_{aer}~~
604 ~~at 9 AERONET stations with satisfactory temporal coverage of data, selected to have~~
605 ~~recorded at least 40 monthly values. In the same figure, these variations are compared~~

606 ~~with corresponding data from MODIS Terra and MODIS Aqua, from the 1x1 degree~~
 607 ~~cells containing the locations of the 9 selected stations. We note that we only perform~~
 608 ~~this analysis in a month only if all three datasets give data for the specific month. It~~
 609 ~~should be noted that the g_{aer} changes for these stations do not refer to the same period~~
 610 ~~but they all ensure a complete enough time period enabling thus the derivation of safe~~
 611 ~~conclusions on how MODIS and AERONET changes compare to each other. At five~~
 612 ~~out of the nine stations (“Barcelona”, “Dhadnah”, “Lecce University”, “Rome Tor~~
 613 ~~Vergata” and “Villefranche”) the temporal tendencies have the same sign for all three~~
 614 ~~databases, with AERONET showing larger trends. Moreover, the trends are~~
 615 ~~statistically significant at the 95% confidence level for “Barcelona” station.~~

616 The overall comparison between satellite and surface g_{aer} data performed in the
 617 scatterplot of Fig. 9 and Table 1 does not allow one to have an insight to how the
 618 comparison behaves spatially, namely how it differs from ~~a one~~ region to another.
 619 This is addressed in Fig. ~~1211~~, showing the comparison of satellite and surface data at
 620 the wavelength of 870 nm separately between MODIS-Terra - AERONET and
 621 MODIS-Aqua – AERONET. For this comparison, we selected AERONET stations
 622 for which there is satisfactory overlap between the time series from AERONET and
 623 the time series from MODIS, namely the number of common days between
 624 AERONET-Terra and AERONET-Aqua is larger than 100. This ~~intentionally selected~~
 625 ~~less strict~~ criterion ~~that the one used in Fig. 11~~ is satisfied by 36 stations for
 626 AERONET-Terra and by 34 for AERONET-Aqua ~~shown in Fig. 121~~. For each
 627 AERONET station we compute the Pearson correlation coefficient between the
 628 station data and the corresponding MODIS-Terra or Aqua data at 870 nm, for the
 629 $1^\circ \times 1^\circ$ cell containing the station. Moreover, there is the information if the trends
 630 between AERONET and either MODIS-Terra or Aqua have the same sign (~~blue~~
 631 ~~color~~) or not (~~red color~~).

632 In the case of the $g_{aer}(\text{AERONET}) - g_{aer}(\text{Terra})$ comparison, at 5 stations, ~~(i.e. in 14% of~~
 633 ~~total 36 stations)~~, the correlation coefficient R is larger than 0.5 ~~(largest R found is~~
 634 ~~0.64 at station “Bahrain”)~~, while at ~~13 stations (36 %) and 264 stations (72%)~~ R is
 635 ~~larger than 0.4 and 0.3, respectively~~ ~~$0.3 < R < 0.5$~~ . ~~The largest R found is 0.64 at station~~
 636 ~~“Bahrain”~~. With respect to the agreement on the sign of the trends, at 24 out of 36
 637 stations (67%) there is a trend sign match and at 12 stations (33%) a mismatch.
 638 ~~Nevertheless, it should be noted that no systematic spatial behaviour, i.e.~~
 639 ~~homogeneous spatial patterns, is found concerning the performance of MODIS-Terra~~

640 g_{aer} against AERONET in terms of either the magnitude of correlation or the
 641 agreement of trends between the satellite and ground datasets. A similar picture
 642 emerges for the comparison $g_{aer} (AERONET) - g_{aer} (Aqua)$. In this case, there are again 5
 643 stations (15% of total 34 stations) with $R > 0.5$ (maximum value $R = 0.61$ again at
 644 “Bahrain”), while at 13 stations (38%) and 24/19 stations (71%) R is larger than 0.4
 645 and 0.3, respectively ~~$0.30 < R < 0.50$~~ . Also, we see that at 22 stations (65%) there is a
 646 trend sign match and at 12 (35%) there is a mismatch ~~(respective percentages equal to~~
 647 ~~65% and 35%)~~.

648

649 **5 Summary and Conclusions**

650 Using satellite data from collection (051) of MODIS-Terra and Aqua data, we
 651 examine the spatiotemporal variations of the aerosol asymmetry parameter (g_{aer}) over
 652 North Africa, the Arabian peninsula and Europe. To our knowledge, this is the first
 653 time that a satellite (MODIS) based dataset of g_{aer} , assessed and evaluated (against
 654 AERONET data), is used for the study region. This is important, since such an
 655 evaluated satellite dataset is very useful for many applications, like radiative transfer
 656 and climate modelling as well as for remote sensing. The advantages of MODIS g_{aer}
 657 data are that:

658 (i) They ensure complete spatial coverage over sea surfaces surrounding Europe,
 659 Mediterranean and Middle East, which is essential for investigating and
 660 understanding physical processes related to aerosols. These processes are
 661 strongly dependent on the aerosol radiative and optical properties, g_{aer} being one
 662 of the three key ones (the other two being aerosol optical thickness and single
 663 scattering albedo). Such a complete spatial coverage is especially required by
 664 radiative transfer and climate models.

665 (ii) They provide with spectral g_{aer} values, at 7 wavelengths from 470 to 2130 nm,
 666 which are of essential importance for radiative transfer models. Such spectrally
 667 resolved aerosol optical properties can induce significant differences in model
 668 computations of aerosol radiative effects (Hatzianastassiou et al., 2007).

669 (iii) They provide a relatively long temporal coverage, i.e. 8 years, which is
 670 significant for examining seasonal and inter-annual cycles and changes of this
 671 aerosol optical property, especially combined with the complete spatial coverage.

672 This is also important since it provides a reasonable statistical bed for attempting
 673 evaluations through comparison against other g_{aer} data like the AERONET.

674 (iv) They constitute the first to know so far satellite based g_{aer} dataset; until now, the
 675 utilized g_{aer} data in modelling or other analyses were taken from in-situ
 676 measurements or aerosol models, which both have their own deficiencies, namely
 677 limited spatial coverage or pure theoretical basis.

678 According to the obtained results, Generally, the largest values of the asymmetry
 679 parameter, indicating the strongest forward scattering of radiation by atmospheric
 680 aerosols, are found over areas with aerosol load being dominated by large size
 681 particles of desert dust (tropical Atlantic, Arabian and Red Seas),. On the contrary,
 682 smaller g_{aer} values are seen where a significant fraction of aerosol load comes from
 683 small size particles of anthropogenic origin, e.g. over the Black Sea. The results are
 684 consistent with the theory and thus prove a good performance of the MODIS retrieval
 685 of aerosol asymmetry parameter. Depending on the area of interest, the seasonal cycle
 686 of the asymmetry parameter varies markedly. More specifically, in areas with
 687 abundance of desert dust particles, the range of intra-annual variation is small, with
 688 the largest values during summer, while in other areas the seasonality is reversed, with
 689 the largest values during the cold season and the smallest during the warm season.
 690 The asymmetry parameter decreases with wavelength, especially when one examines
 691 its spatially minimum values, while this decrease is weaker for the larger g_{aer} values,
 692 corresponding to the presence of coarser particles.

693 The seasonal fluctuation is more pronounced with increasing wavelength in the
 694 examined regions, which is attributed to the different spectral behaviour of the
 695 asymmetry parameter for small and large particles. With respect to the inter-annual
 696 variability of the asymmetry parameter, we did not discern very important either
 697 increasing or decreasing tendencies, with absolute changes smaller than 0.04 in any
 698 case. On the other hand, we found opposing tendencies for the two satellite datasets.

699 MODIS-Terra observes mostly increasing tendencies, while Aqua gives also
 700 extensive-a few regions with decreasing tendencies. Generally, the largest intra-annual
 701 and inter-annual variations are seen over the Black Sea, while the smallest over the
 702 tropical Atlantic. However, some strong trends (especially from Terra) may be due to
 703 calibration drift errors, which may be addressed in collection 006. Along these lines
 704 we performed some preliminary comparisons between 051 and 006
 705 Ångström Exponent trends from Aqua, which ensured that AE and g_{aer} are

706 very closely anti-correlated. These preliminary results, show that 051 Aqua AE trends
707 resemble very closely the 006 trends, supporting that the g_{aer} trends from collection
708 051 (at least for Aqua) reported in this study are credible.

709 The 051 MODIS g_{aer} data is not a retrieved but a derived MODIS parameter. Given
710 that the retrieval is strongly dependent on the assumptions made, namely on the
711 aerosol modes used, uncertainties can be associated with its use in radiative transfer
712 modeling. In order to examine these uncertainties, the g_{aer} data were compared with
713 051 AE data for the same period. The results from the comparison showed a strong
714 anti-correlation (coefficient higher than 0.7-0.8) proving the consistency and
715 reasonably safe use of g_{aer} data in modeling studies, at least to the same degree with
716 MODIS AE data in modeling and other analyses. The correlation is even higher over
717 sea areas characterized by stronger presence of fine aerosols, like the Black Sea, the
718 Persian Gulf or the North Sea. This confidence is further strengthened by the small
719 identified uncertainties related with the use of collection 051 instead of 006 MODIS
720 g_{aer} data reported in the previous paragraph. This was obtained indirectly based on the
721 use of AE data of both collections since g_{aer} data are not yet available in collection
722 006.

723 We compare satellite data with surface data from the AERONET, in order to further
724 validate the reliability of the former. ~~The quantitative comparison is very useful, since~~
725 ~~satellite data provide broad geographical coverage and are very important in any study~~
726 ~~related to aerosols and their climate impact. The disagreement with surface stations~~
727 ~~can give insights in the resulting errors.~~ Through the examination of frequency
728 distributions of daily g_{aer} , a shift of satellite data towards larger values relative to
729 surface data becomes apparent. This finding is more pronounced for g_{aer} over Europe,
730 while the North African, Arabian peninsula values are more in agreement. Moreover,
731 the smallest g_{aer} values originate from particles from Europe, because of the
732 generation of smaller size particles by industrial activities and biomass burning.

733 ~~In this work w~~We present scatter plots of daily g_{aer} values between MODIS-Terra,
734 MODIS-Aqua, and AERONET, which show moderate agreement between satellite
735 data at 470 nm and surface data at 440 nm, with small correlation coefficients ($R < 0.3$)
736 and a slight underestimation by MODIS. Slightly better agreement was noted at larger
737 wavelengths, but still without reaching very satisfactory levels ($R < 0.47$).
738 Nevertheless, during spring and summer, satellite and surface measurements tend to
739 agree more. Finally, for the comparisons at 660/675 and 870 nm, we report an

740 overestimation of g_{aer} by MODIS compared to AERONET, ~~as expected because of the~~
741 ~~less steep decrease of g_{aer} with wavelength of MODIS.~~

742 When examined at the local scale, i.e. station by station, the MODIS g_{aer} data agree
743 reasonably and for some stations better than in overall, but still not very well, with
744 those of AERONET. This analysis, based on 36 and 34 AERONET stations ensuring
745 at least 100 common days with MODIS-Terra and Aqua, respectively, shows that in
746 36 and 38% of stations, respectively, the MODIS data have correlation coefficients
747 larger than 0.4 (reaching values up to 0.64), while in about 65% of stations the trends
748 of g_{aer} from MODIS and AERONET have the same sign. Nevertheless, the magnitude
749 of correlation coefficients or the agreement between trends of g_{aer} from the satellite
750 and ground datasets do not exhibit a systematic (homogeneous) spatial pattern.

751 ~~We extract pairs of daily Terra-AERONET and Aqua-AERONET values at stations~~
752 ~~with at least 100 common days. At 21 of 36 stations (Terra-AERONET comparison)~~
753 ~~and at 19 of 34 stations (Aqua-AERONET comparison) we derive $0.3 < R < 0.5$, while~~
754 ~~at 5 stations in both cases, the correlation coefficients are larger than 0.5. Finally, as~~
755 ~~far as the signs of temporal trends are concerned, we determine agreement in 67%~~
756 ~~(Terra-AERONET comparison) and in 65% of stations (Aqua-AERONET~~
757 ~~comparison).~~

758 Our results can offer an interesting way to assess the uncertainty induced by the use of
759 such satellite g_{aer} data in climate and radiative transfer models that compute aerosol
760 radiative and climate effects. Based on an overall assessment of satellite MODIS g_{aer}
761 through detailed comparisons against ground AERONET data, it appears that in
762 overall MODIS performs satisfactorily in terms of magnitude of g_{aer} values. This is
763 indicated by the computed biases, which are smaller than 5% with respect to MODIS
764 values, with better performance at smaller wavelengths. The root mean squared errors
765 vary within the range 5-10% again being smaller for smaller wavelengths. These
766 results indicate an uncertainty of MODIS g_{aer} data over the study region up to of 10%
767 at maximum. Previous analyses and sensitivity studies for the same study region
768 (Papadimas et al., 2012) have shown that such g_{aer} uncertainties can induce
769 modifications of aerosol direct radiative effects (DREs) which are equal to 30% at the
770 top-of-atmosphere (TOA) and 1% in the atmosphere and 10% at the surface, at
771 maximum. Therefore, the uncertainty associated with the use of MODIS g_{aer} is larger
772 as to any aerosol related physical process taking place at TOA, namely planetary
773 cooling or warming and its magnitude, smaller for processes at the Earth's surface,

774 e.g. surface cooling and very small for aerosol processes and feedbacks in the
775 atmosphere, like the aerosol semi-direct effect and its implications. Results from the
776 same previous analysis (Papadimas et al., 2012) proved that the exact magnitude of
777 MODIS g_{aer} DRE uncertainty can be estimated by simple linear equations relating
778 DREs and g_{aer} , separately given for TOA, atmosphere and surface.

779 The results of the present analysis are useful since they assess for the first time the
780 performance of satellite based products of aerosol asymmetry parameter over broad
781 regions of special climatic interest. ~~Our results can offer an interesting way to assess~~
782 ~~the uncertainty induced by the use of such satellite g_{aer} data in climate and radiative~~
783 ~~transfer models that compute aerosol radiative and climate effects.~~ The obtained
784 results are relatively satisfactory given the difficulties encountered by satellite
785 retrieval algorithms due to the different assumptions they made. Nevertheless, our
786 results and identified weaknesses remind that users should be aware of the g_{aer}
787 uncertainties and their consequences. The identified weaknesses may provide an
788 opportunity to improve such satellite retrievals of aerosol asymmetry parameter in
789 forthcoming data products like those of MODIS C006. The increased temporal
790 coverage of g_{aer} data, combined with the continued operation of MODIS, is expected
791 to make possible the building of the first real satellite climatology of this important
792 aerosol optical property.

794 **76 Acknowledgments**

795 This research has been co-financed by the European Union (European Social Fund –
796 ESF) and Greek national funds through the operational programme “Education and
797 Lifelong Learning” of the National Strategic Reference Framework (NSRF) –
798 Research Funding Program: THALES. Investing in knowledge society through the
799 European Social Fund. The Collection 051005 MODIS-Terra data were obtained from
800 NASA’s Level 1 and Atmosphere Archive and Distribution System (LAADS) website
801 (<ftp://ladsweb.nascom.nasa.gov/>). We would like to thank the principal investigators
802 maintaining the AERONET sites used in the present work.

803

804 **References**

- 805 [Alonso-Pérez S., Cuevas E., Querol X., Guerra J. C., and Pérez C. \(2012\). African dust source](#)
 806 [regions for observed dust outbreaks over the Subtropical Eastern North Atlantic region,](#)
 807 [above 25°N, J. Arid Environ., 79, 100-109, doi:10.1016/j.jaridenv.2011.11.013.](#)
- 808 Barnaba F. and G. P. Gobbi: Aerosol seasonal variability over the Mediterranean region and
 809 relative impact of maritime, continental and Saharan dust particles over the basin from
 810 MODIS data in the year 2001, Atmospheric Chemistry and Physics, 4, 4285 - 4337, SRef-
 811 ID: 1680-7375/acpd/2004-4-4285SRef-ID: 1680-7375/acpd/2004-4-4285, 2004.
- 812 [Barnaba F., Angelini F., Curci G., and Gobbi G. P. \(2011\), An important fingerprint of](#)
 813 [wildfires on the European aerosol load, Atmos. Chem. Phys., 11, 10,487–10,501.](#)
- 814 [Bovchaliuk A., Milinevsky G., Danylevsky V., Goloub P., Dubovik O., Holdak A., and](#)
 815 [Sosonkin, M. \(2013\). Variability of aerosol properties over Eastern Europe observed from](#)
 816 [ground and satellites in the period from 2003 to 2011. Atmos. Chem. Phys., 13, 6587-6602](#)
- 817 [Bréon F.-M., Vermeulen A., and Descloitres J. \(2011\). An evaluation of satellite aerosol](#)
 818 [products against sunphotometers measurements, Remote Sens. Environ., 115, 3102–3111.](#)
- 819 Chubarova, N. Y.: Seasonal distribution of aerosol properties over Europe and their impact on
 820 UV irradiance, Atmos. Meas. Tech., 2, 593–608, doi:10.5194/amt-2-593-2009, 2009.
- 821 Di Iorio, T., A. di Sarra, W. Junkermann, M. Cacciani, G. Fiocco, and D. Fua, Tropospheric
 822 aerosols in the Mediterranean: 1. Microphysical and optical properties, J. Geophys. Res.,
 823 108(D10), 4316, doi:10.1029/2002JD002815, 2003
- 824 Dubovik, Oleg, Brent Holben, Thomas F. Eck, Alexander Smirnov, Yoram J. Kaufman,
 825 Michael D. King, Didier Tanré, Ilya Slutsker, 2002: Variability of Absorption and Optical
 826 Properties of Key Aerosol Types Observed in Worldwide Locations. *J. Atmos. Sci.*, **59**,
 827 590–608.
- 828 Dubovik, O. and M. D. King, 2000: A flexible inversion algorithm for retrieval of aerosol
 829 optical properties from Sun and sky radiance measurements," J. Geophys. Res., 105, 20
 830 673-20 696.
- 831 [Engelstaedter S., Tegen I., and Washington R. \(2006\). North African dust emissions and](#)
 832 [transport, Earth-Sci. Revi., 79\(1-2\), 73-100.](#)
- 833 Fotiadi, A., E. Drakakis, N. Hatzianastassiou, C. Matsoukas, K. G. Pavlakis, D.
 834 Hatzidimitriou, E. Gerasopoulos, N. Mihalopoulos, and I. Vardavas (2006), Aerosol
 835 physical and optical properties in the eastern Mediterranean Basin, Crete, from Aerosol
 836 Robotic Network data, Atmos. Chem. Phys., 6, 5399– 5413.
- 837 Gerasopoulos, E., Kouvarakis, G., Babasakalis, P., Vrekoussis, M., Putaud, J. P., and
 838 Mihalopoulos, N.: Origin and variability of particulate matter (PM10) mass concentrations
 839 over the Eastern Mediterranean, Atmos. Environ., 40, 4679–4690, 2006.

- 840 [Ginoux P, Prospero J. M., Gill T. E., Hsu C. N., Zhao M., \(2012\). Global-scale attribution of](#)
841 [anthropogenic and natural dust sources and their emission rates based on MODIS Deep](#)
842 [Blue aerosol products. Rev. Geophys. 50, RG3005. doi:10.1029/2012RG000388.](#)
- 843 Gkikas, A., Hatzianastassiou, N., and Mihalopoulos, N.: Study and characterization of aerosol
844 episodes in the Mediterranean basin for the 7-year period 2000–2007 based on MODIS
845 data, European Aerosol Conference, Greece, Thessaloniki, 24–29 August 2008.
- 846 Gkikas, A., Hatzianastassiou, N., and Mihalopoulos, N.: Aerosol events in the broader
847 Mediterranean basin based on 7-year (2000–2007) MODIS C005 data, Ann. Geophys., 27,
848 3509–3522, doi:10.5194/angeo-27-3509-2009, 2009.
- 849 Gkikas, A., Houssos, E., Hatzianastassiou, N., Papadimas, C. and Bartzokas, A. (2011),
850 Synoptic conditions favouring the occurrence of aerosol episodes over the broader
851 Mediterranean basin. Q.J.R. Meteorol. Soc.. doi: 10.1002/qj.978.
- 852 [Gkikas, A., Hatzianastassiou, N., Mihalopoulos, N., Katsoulis, V., Kazadzis, S., Pey, J., and](#)
853 [Torres, O. \(2013\). The regime of intense desert dust episodes in the Mediterranean based](#)
854 [on contemporary satellite observations and ground measurements. Atmos. Chem. Phys.,](#)
855 [13, 12135-12154.](#)
- 856 [Gkikas A., Houssos E. E., Lolis C. J., Bartzokas A., Mihalopoulos N., and Hatzianastassiou](#)
857 [N. \(2014\), Atmospheric circulation evolution related to desert-dust episodes over the](#)
858 [Mediterranean. Quart. J. Roy. Meteorol. Soc., 690, 1634-1645.](#)
- 859 Goloub, P., and O. Arino, 2000: Verification of the consistency of POLDER aerosol index
860 over land with ATSR-2 fire product. Geophys. Res. Lett., 27, 899–902.
- 861 Graßl, H.: Possible changes of planetary albedo due to aerosol particles, in Man's Impact on
862 Climate, edited by: W. Bach, J. Pankrath, and W. Kellogg, Elsevier, New York, 1979.
- 863 Hansen, J., Sato, M., and Ruedy, R.: Radiative forcing and climate response, J. Geophys.
864 Res., 102, 6831–6864, 1997.
- 865 Hatzianastassiou, N., B. Katsoulis, I. Vardavas: Sensitivity analysis of aerosol direct radiative
866 forcing in ultraviolet - visible wavelengths and consequences for the heat budget, Tellus,
867 56b, 368 - 381, 2004.
- 868 Hatzianastassiou, N., A. Gkikas, N. Mihalopoulos, O. Torres, and B. D. Katsoulis: Natural
869 versus anthropogenic aerosols in the eastern Mediterranean basin derived from multiyear
870 TOMS and MODIS satellite data, J. Geophys. Res., 114, D24202,
871 doi:10.1029/2009JD011982, 2009.
- 872 Hatzianastassiou, N., Matsoukas, C., Drakakis, E., Stackhouse Jr., P. W., Koepke, P.,
873 Fotiadi, A., Pavlakis, K. G., and Vardavas, I.: The direct effect of aerosols on solar
874 radiation based on satellite observations, reanalysis datasets, and spectral aerosol optical
875 properties from Global Aerosol Data Set (GADS), Atmos. Chem. Phys., 7, 2585-2599,
876 doi:10.5194/acp-7-2585-2007, 2007.

- 877 Haywood, J.M., and O. Boucher, 2000: Estimates of the direct and indirect radiative forcing
878 due to tropospheric aerosols: A review. *Rev. Geophys.*, 38, 513–543.
- 879 Heishman, J. (1999), Commanding Officer, Forecaster's Handbook, U.S. Navy Cent.
880 Meteorol. and Oceanogr. Cent., Manama, Bahrain.
- 881 Holben B.N., T.F. Eck, I. Slutsker, D. Tanré, J.P. Buis, A. Setzer, E. Vermote, J.A. Reagan,
882 Y. Kaufman, T. Nakajima, F. Lavenu, I. Jankowiak, and A. Smirnov, 1998: AERONET -
883 A federated instrument network and data archive for aerosol characterization, *Rem. Sens.*
884 *Environ.*, 66, 1-16.
- 885 Ichoku C., D. Allen Chu, Shana Mattoo, Yoram J. Kaufman, Lorraine A. Remer, Didier Tanré,
886 Ilya Slutsker, and Brent N. Holben: A spatio-temporal approach for global validation and
887 analysis of MODIS aerosol products. *GEOPHYSICAL RESEARCH LETTERS*, VOL. 29,
888 NO. 12, 10.1029/2001GL013206, 2002.
- 889 IPCC, 2007: *Climate Change 2007: The Physical Science Basis*. Contribution of Working
890 Group I to the Fourth Assessment Report of the Intergovernmental Panel on Climate
891 Change [Solomon, S., D. Qin, M. Manning, Z. Chen, M. Marquis, K.B. Averyt, M. Tignor
892 and H.L. Miller (eds.)]. Cambridge University Press, Cambridge, United Kingdom and
893 New York, NY, USA.
- 894 IPCC, 2013: *Climate Change 2013: The Physical Science Basis*. Contribution of Working
895 Group I to the Fifth Assessment Report of the Intergovernmental Panel on Climate Change
896 [Stocker, T.F., D. Qin, G.-K. Plattner, M. Tignor, S.K. Allen, J. Boschung, A. Nauels, Y.
897 Xia, V. Bex and P.M. Midgley (eds.)]. Cambridge University Press, Cambridge, United
898 Kingdom and New York, NY, USA, 1535 pp.
- 899 [Joseph J. H., Wiscombe W. J., and Weinman, J. A. \(1976\). The delta-Eddington](#)
900 [approximation for radiative flux transfer. *J. Atmos. Sci.*, 33, 2452–2459.](#)
- 901 Jianrong Bi, Jianping Huang, Qiang Fu, XinWanga, Jinsen Shi , Wu Zhang , Zhongwei
902 Huang, Beidou Zhang: Toward characterization of the aerosol optical properties over
903 Loess Plateau of Northwestern China. *Journal of Quantitative Spectroscopy & Radiative*
904 *Transfer* 112 (2011) 346–360.
- 905 [Kalapureddy, M. C. R., D. G. Kaskaoutis, P. Ernest Raj, P. C. S. Devara, H. D. Kambezidis,](#)
906 [P. G. Kosmopoulos, and P. T. Nastos \(2009\), Identification of aerosol type over the](#)
907 [Arabian Sea in the premonsoon season during the Integrated Campaign for Aerosols,](#)
908 [Gases and Radiation Budget \(ICARB\), *J. Geophys. Res.*, 114, D17203,](#)
909 [doi:10.1029/2009JD011826.](#)
- 910 Kalivitis, N., Gerasopoulos, E., Vrekoussis, M., Kouvarakis, G., Kubilay, N.,
911 Hatzianastassiou, N., Vardavas, I., and Mihalopoulos, N.: Dust transport over the eastern
912 Mediterranean derived from TOMS, AERONET and surface measurements, *J. Geophys.*
913 *Res.*, 112, D03202, doi:10.1029/2006JD007510, 2007.

- 914 Kaufman, Y. J., D. Tanré, L. A. Remer, E. F. Vermote, A. Chu, and B. N. Holben:
915 Operational remote sensing of tropospheric aerosol over land from EOS moderate
916 resolution imaging spectroradiometer, *J. Geophys. Res.*, 102, 17,051– 17,067, 1997.
- 917 Kinne, S., D. O'Donnell, P. Stier, S. Kloster, K. Zhang, H. Schmidt, S. Rast, M. Giorgetta, T.
918 F. Eck, and B. Stevens (2013), MAC-v1: A new global aerosol climatology for climate
919 studies, *J. Adv. Model. Earth Syst.*, 5, 704–740, doi:10.1002/jame.20035.
- 920 [Kishcha, P., A. M. da Silva, B. Starobinets, C. N. Long, O. Kalashnikova, and P. Alpert,](#)
921 [Meridional distribution of aerosol optical thickness over the tropical Atlantic Ocean,](#)
922 [Atmos. Chem. Phys. Discuss., 14, 23309-23339, 2014.](#)
- 923 Koepke, P., M. Hess, I. Schult, and E. P. Shettle: Global aerosol data set, Rep. No. 243, Max-
924 Planck Institut fuer Meteorologie, Hamburg, Germany, 44 pp., 1997.
- 925 [Kondratyev, K. Y. 1999. Climatic effects of aerosols and clouds. Springer, New York.](#)
- 926 [Kutiel H., Furman, H., \(2003\). Dust storms in the Middle East: sources of origin and their](#)
927 [temporal characteristics. Indoor Built Environ.](#) 12, 419–426.
- 928 Lelieveld, J., et al. (2002), Global air pollution crossroads over the Mediterranean, *Science*,
929 298, 794– 799, doi:10.1126/science.1075457.
- 930 [Levy, R. C., Remer, L. A., Kleidman, R. G., Mattoo, S., Ichoku, C., Kahn, R., and](#)
931 [Eck, T. F.: Global evaluation of the Collection 5 MODIS dark-target aerosol](#)
932 [products over land, Atmos. Chem. Phys., 10, 10399-10420, doi:10.5194/acp-10-](#)
933 [10399-2010, 2010.](#)
- 934 Lohmann U., Feichter, J. [2005] Global indirect aerosol effects: A review . *Atmos. Chem.*
935 *Phys.*, 5, 715-737.
- 936 [Miller S. D., Kuciauskas A. P., Liu M., Ji Q., Reid J. S., Breed D. W. Walker A. L., and](#)
937 [Mandoos A. A.. \(2008\). Haboob dust storms of the southern Arabian Peninsula, J.](#)
938 [Geophys. Res., 113, D01202, doi:10.1029/2007JD008550.](#)
- 939 [Nabat P., Somot S., Malle, M., Chiapello I., Morcrette J. J., Solmon F., Szopa S., Dulac F.,](#)
940 [Collins W., Ghan S., Horowitz L. W., Lamarque J. F., Lee Y. H., Naik V., Nagashima T.,](#)
941 [Shindell D., and Skeie R. \(2013\), A 4-D climatology \(1979–2009\) of the monthly](#)
942 [tropospheric aerosol optical depth distribution over the Mediterranean region from a](#)
943 [comparative evaluation and blending of remote sensing and model products. Atmos. Meas.](#)
944 [Tech., 6, 1287–1314.](#)
- 945 Lyamani, H., F. J. Olmo, A. Alca'ntara, and L. Alados-Arboledas (2006), Atmospheric
946 aerosols during the 2003 heat wave in southeastern Spain. I: Spectral optical depth, *Atmos.*
947 *Environ.*, 40, 6453 – 6464, doi:10.1016/j.atmosenv.2006.04.048.
- 948 Papadimas, C. D., N. Hatzianastassiou, N. Mihalopoulos, X. Querol, and I.
949 Vardavas (2008), Spatial and temporal variability in aerosol properties over the
950 Mediterranean basin based on 6-year (2000–2006) MODIS data, *J. Geophys. Res.*, 113,
951 D11205, doi:10.1029/2007JD009189.

- 952 [Papadimas C. D., Hatzianastassiou N., Matsoukas C., Kanakidou M., Mihalopoulos N.,](#)
 953 [and Vardavas, I. \(2012\). The direct effect of aerosols on solar radiation over the](#)
 954 [broader Mediterranean basin. *Atmos. Chem. Phys.*, 12, 7165-7185.](#)
- 955 Pace, G., A. di Sarra, Meloni, D., Piacentino, S., and Chamard, P.: Aerosol optical properties
 956 at Lampedusa (Central Mediterranean). 1. Influence of transport and identification of
 957 different aerosol types, *Atmos. Chem. Phys.*, 6, 697–713, 2006, [www.atmos-chem-](http://www.atmos-chem-phys.net/6/697/2006/)
 958 [phys.net/6/697/2006/](http://www.atmos-chem-phys.net/6/697/2006/).
- 959 Pandithurai, R. T. Pinker, P. C. S. Devara, T. Takamura, K. K. Dani, Seasonal asymmetry in
 960 diurnal variation of aerosol optical characteristics over Pune, western India, *J. Geophys.*
 961 *Res.*, 112, D8, DOI: 10.1029/2006JD007803, 2007.
- 962 [Pilinis, Ch., Pandis, S. N. and Seinfeld, J. H. 1996. Sensitivity of direct climate forcing by](#)
 963 [anthropogenic aerosols to aerosol size distribution and composition. *J. Geophys. Res.* 100,](#)
 964 [18 739–18 754.](#)
- 965 Prospero, J., P. Ginoux, O. Torres, and S. E. Nicholson (2002), Environmental
 966 Characterization of Global sources of atmospheric soil dust derived from the NIMBUS-7
 967 TOMS absorbing aerosol product, *Rev. Geophys.*, 40(1), 1002,
 968 doi:10.1029/20000GR000095.
- 969 [Rahul, PRC and Salvekar, PS and Devara, PCS \(2008\) Aerosol optical depth variability over](#)
 970 [Arabian Sea during drought and normal years of Indian monsoon. *Geophysical Research*](#)
 971 [Letters, 35 \(22\).](#)
- 972 [Rashki A., Kaskaoutis D. G., de W. Rautenbach C. J., Eriksson P. G., Qiang M, and Gupta](#)
 973 [P., \(2012\). Dust storms and their horizontal dust loading in the Sistan region, Iran. *Aeolian*](#)
 974 [Res 5: 51–62.](#)
- 975 [Rashki A., Kaskaoutis D. G., Eriksson P. G., de W. Rautenbach C. J., Flamant C., Abdi](#)
 976 [Vishkaee F., \(2014\). Spatio-temporal variability of dust aerosols over the Sistan region in](#)
 977 [Iran based on satellite observations. *Nat. Hazards*, doi: 10.1007/s11069-013-0927-0.](#)
- 978 [Remer L.A., Tanre D., Kaufman Y.J., Levy R, and Matoo S.: Algorithm for Remote Sensing](#)
 979 [of Tropospheric Aerosol from MODIS: Collection 005, 2006,](#)
 980 http://modis.gsfc.nasa.gov/data/atbd/atbd_mod02.pdf.
- 981 Remer L.A., Kaufman Y.J., Tanre D. and co-authors: The MODIS aerosol algorithm,
 982 products, and validation, *J. Atmos. Sci.*, 62: 947-973, 2005.
- 983 Remer LA, Kleidman RG, Levy RC, Kaufman YJ, Tanre D, Mattoo S, Martins JV, Ichoku
 984 C, Koren I, Yu H, Holben BN. 2008. Global aerosol climatology from the MODIS satellite
 985 sensors. *Journal of Geophysical Research* 113: D14S07, DOI: 10.1029/2007JD009661.
- 986 Satheesh, S. K., V. Ramanathan, X. Li-Jones, J. M. Lobert, I. A. Podgorny, J. M. Prospero, B.
 987 N. Holben, and N. G. Loeb, A model for the natural and anthropogenic aerosols over the
 988 tropical Indian Ocean derived from Indian Ocean Experiment data, *J. Geophys. Res.*, 104,
 989 27,421–27,440, 1999.

- 990 | [Satheesh, S. K., K. Krishna Moorthy, Y. J. Kaufman, and T. Takemura, Aerosol optical depth,](#)
991 | [physical properties and radiative forcing over the Arabian Sea, Meteorology and](#)
992 | [Atmospheric Physics, Volume 91, Issue 1, pp 45-62, 2006.](#)
- 993 | Savoie, D. L., J. M. Prospero, and R. T. Nees, Nitrate, nonsea-salt sulfate, and mineral
994 | aerosol over the northwestern Indian Ocean, *J. Geophys. Res.*, 92, 933–942, 1987.
- 995 | Sciare, J., H. Bardouki, C. Moulin, and N. Mihalopoulos (2003), Aerosol sources and their
996 | contribution to the chemical composition of aerosols in the Eastern Mediterranean Sea
997 | during summertime, *Atmos. Chem. Phys.*, 3, 291–302, SRef-ID:1680 – 7324/acp/2003–3-
998 | 291.
- 999 | [Smirnov A., Holben B. N., Dubovik O., O'Neill N. T., Eck T. F., Westphal D. L., Goroch A.](#)
1000 | [K., Pietras C., and Slutsker I, 2002a: Atmospheric Aerosol Optical Properties in the](#)
1001 | [Persian Gulf. *J. Atmos. Sci.*, 59, 620–634, doi: http://dx.doi.org/10.1175/1520-](#)
1002 | [0469\(2002\)059<0620:AAOPIT>2.0.CO;2.](#)
- 1003 | Smirnov, A., B. N. Holben, Y. J. Kaufman, O. Dubovik, T. F. Eck, I. Slutsker, C. Pietras, and
1004 | R. N. Halthore, 2002b: Optical properties of atmospheric aerosol in maritime
1005 | environments. *J. Atmos. Sci.*, 59, 501–523.
- 1006 | ~~Smirnov, and Coauthors, 2002a: Atmospheric aerosol optical properties in the Persian Gulf. *J.*~~
1007 | ~~*Atmos. Sci.*, 59, 620–634.~~
- 1008 | Smirnov, A., B. N. Holben, T. F. Eck, I. Slutsker, B. Chatenet, and R. T. Pinker, 2002c:
1009 | Diurnal variability of aerosol optical depth observed at AERONET (Aerosol Robotic
1010 | Network) sites, *Geophys. Res. Lett.*, 29, 23, 2115, doi:10.1029/2002GL016305.
- 1011 | Tanré, D., Y. J. Kaufman, M. Herman, and S. Mattoo: Remote sensing of aerosol properties
1012 | over oceans using the MODIS/EOS spectral radiances, *J. Geophys. Res.*, 102, 16,971–
1013 | 16,988, 1997.
- 1014 | Tindale, N. W., and P. P. Pease, Aerosols over the Arabian Sea: Atmospheric transport
1015 | pathways and concentrations of dust and sea salt, *Deep Sea Res.*, 46, 1577–1595, 1999.
- 1016 | Yu, H., Dickinson, R. E., Chin, M., Kaufman, Y. J., Holben, B. N. Geogdzhayev, I. V., and
1017 | Mishchenko, M. I.: Annual cycle of global distributions of aerosol optical depth from
1018 | integration of MODIS retrievals and GOCART model simulations, *J. Geophys. Res.*, 108,
1019 | 4128, doi:10.1029/2002JD002717, 2003.
- 1020 | Zdun, A., A. Rozwadowska and S. Kratzer, 2011. Seasonal variability in the optical
1021 | properties of Baltic aerosols, *Oceanologia*, 53(1), 7-34.
- 1022 | [Zuluaga, M. D., P. J. Webster, and C. D. Hoyos \(2012\), Variability of aerosols in the](#)
1023 | [tropical Atlantic Ocean relative to African Easterly Waves and their relationship with](#)
1024 | [atmospheric and oceanic environments, *J. Geophys. Res.*, 117, D16207,](#)
1025 | [doi:10.1029/2011JD017181.](#)
- 1026

1027 **Table 1.** Correlation coefficients (R), mean bias, root mean squared error (RMSE) and
 1028 the slope and intercept values of applied linear regression fits between MODIS and
 1029 AERONET g_{aer} data. The statistical parameters are given separately for the pairs of
 1030 wavelengths: (i) 470 nm (MODIS) and 440 nm (AERONET), (ii) 660 nm (MODIS)
 1031 and 675nm (AERONET) and (iii) 870 nm (MODIS and AERONET). The statistical
 1032 parameters are also given separately for winter, spring, summer and autumn. ^a

1033

1034 *MODIS-Terra*

1035

		R	Bias*	RMSE	Slope	Intercept
year	470-440	0.25	2×10^{-4}	0.045	0.36	0.45
	660-675	0.41	-0.028	0.060	0.55	0.32
	870	0.47	-0.035	0.070	0.60	0.29
W i n t e r	470-440	0.20	4.5×10^{-4}	0.046	0.26	0.53
	660-675	0.35	-0.033	0.056	0.41	0.42
	870	0.41	-0.053	0.057	0.40	0.43
Sp r i n g	470-440	0.27	-5×10^{-4}	0.046	0.40	0.43
	660-675	0.44	-0.023	0.060	0.63	0.27
	870	0.50	-0.026	0.071	0.67	0.24
Su m m e r	470-440	0.33	-0.002	0.044	0.51	0.35
	660-675	0.48	-0.031	0.061	0.71	0.22
	870	0.54	-0.030	0.077	0.79	0.16
Au t u m n	470-440	0.21	0.003	0.044	0.30	0.50

^aThe reported correlation coefficients and slopes may be biased low, because we did not include in our analysis the unknown AERONET errors.

660-675	0.33	-0.027	0.059	0.45	0.38
870	0.41	-0.035	0.068	0.53	0.34

1036

1037

1038 *MODIS-Aqua*

1039

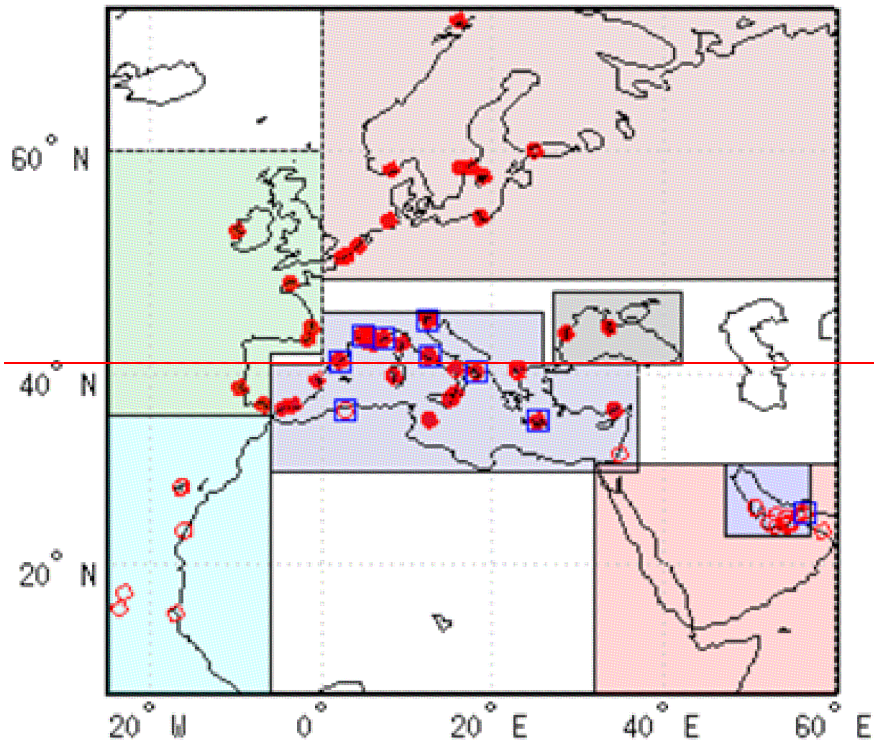
		R	Bias*	RMSE	Slope	Intercept
	470-440	0.27	0.018	0.047	0.41	0.40
	660-675	0.42	-0.005	0.062	0.61	0.26
	870	0.46	-0.015	0.072	0.61	0.26
W i n t e r	470-440	0.25	0.024	0.049	0.36	0.43
	660-675	0.39	-0.001	0.062	0.55	0.30
	870	0.43	-0.021	0.068	0.51	0.33
Sp rin g	470-440	0.29	0.015	0.048	0.45	0.38
	660-675	0.45	-0.003	0.064	0.70	0.20
	870	0.50	-0.007	0.076	0.71	0.19
Su m me r	470-440	0.35	0.014	0.045	0.55	0.30
	660-675	0.50	-0.012	0.060	0.72	0.19
	870	0.53	-0.018	0.074	0.73	0.19
Au t u m n	470-440	0.20	0.021	0.047	0.30	0.47
	660-675	0.32	-0.003	0.061	0.46	0.36
	870	0.37	-0.014	0.069	0.48	0.34

1040

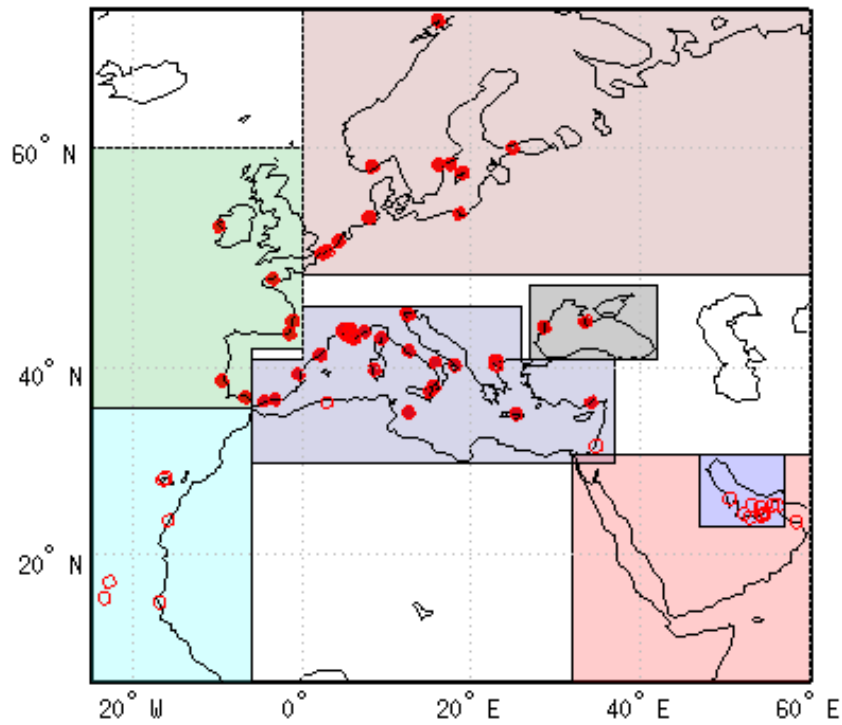
1041

* $g_{aer(AERONET)} - g_{aer(MODIS)}$

1042



1043



1044

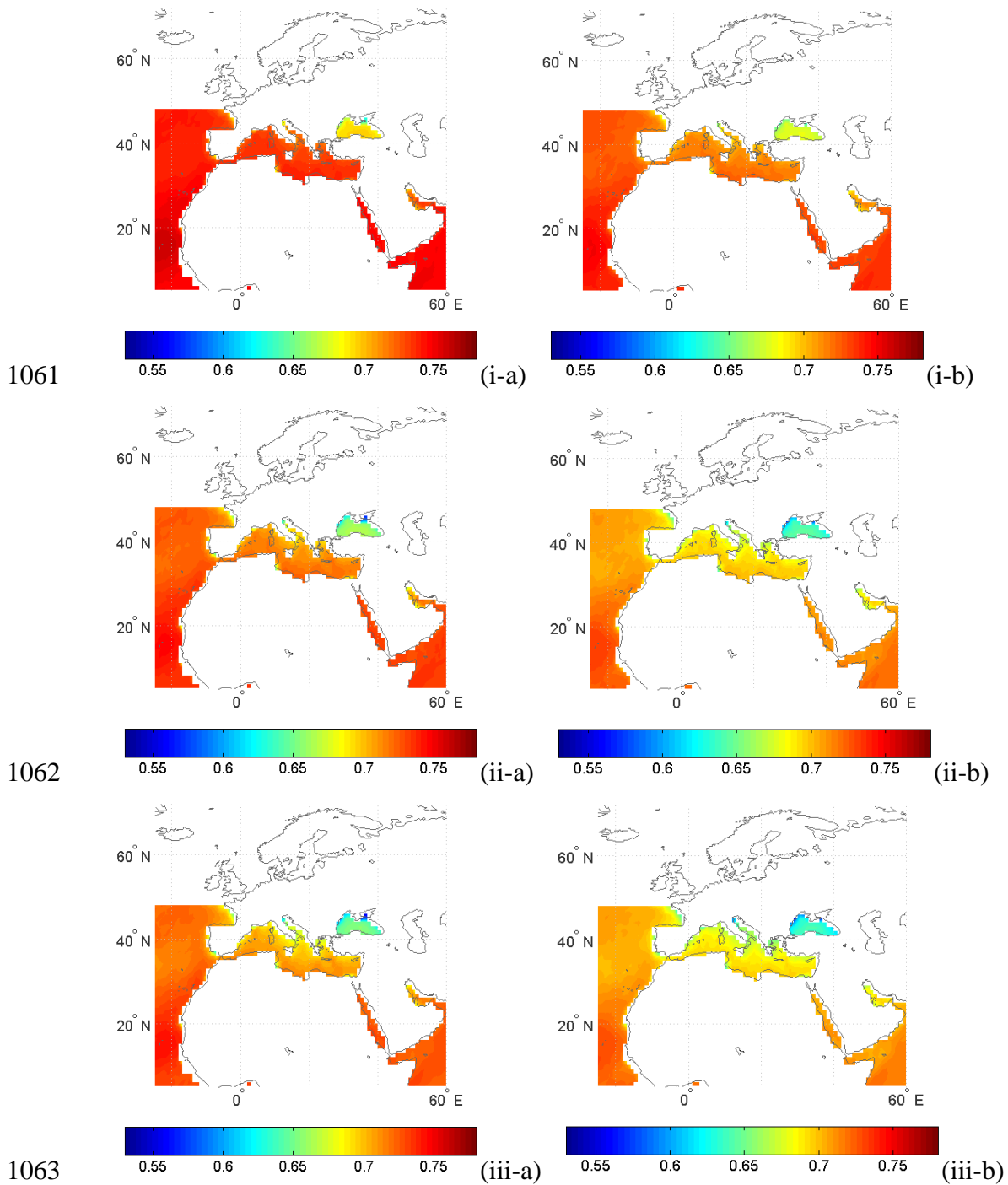
1045

1046 **Figure 1.** The study region (5°N–70°N, 25°W–60°E) and the location of 69
 1047 AERONET stations used for validation of MODIS satellite aerosol asymmetry
 1048 parameter (g_{aer}) data. Solid red circles denote stations located in Europe and hollow
 1049 red circles are stations in Africa, Middle East and the Arabian peninsula. ~~The nine~~
 1050 stations inscribed in blue squares have high AERONET and MODIS g_{aer} data

1051 ~~availability and therefore selected for examining g_{aer} temporal tendencies. Also shown~~
1052 ~~are seven sub-regions selected for studying the seasonal variation of g_{aer} . Comparison~~
1053 ~~between HAC and MODIS total aerosol optical depth at 550nm. Global seasonal~~
1054 ~~distribution of relative percentage differences $((HAC - MODIS)/MODIS \cdot \%)$ for: (a)~~
1055 ~~winter (December January February), (b) spring (March April May), (c) summer~~
1056 ~~(June July August) and (d) autumn (September October November). White shaded~~
1057 ~~areas correspond to cases for which MODIS AOD values are missing or do not~~
1058 ~~qualify for the averaging threshold.~~

1059

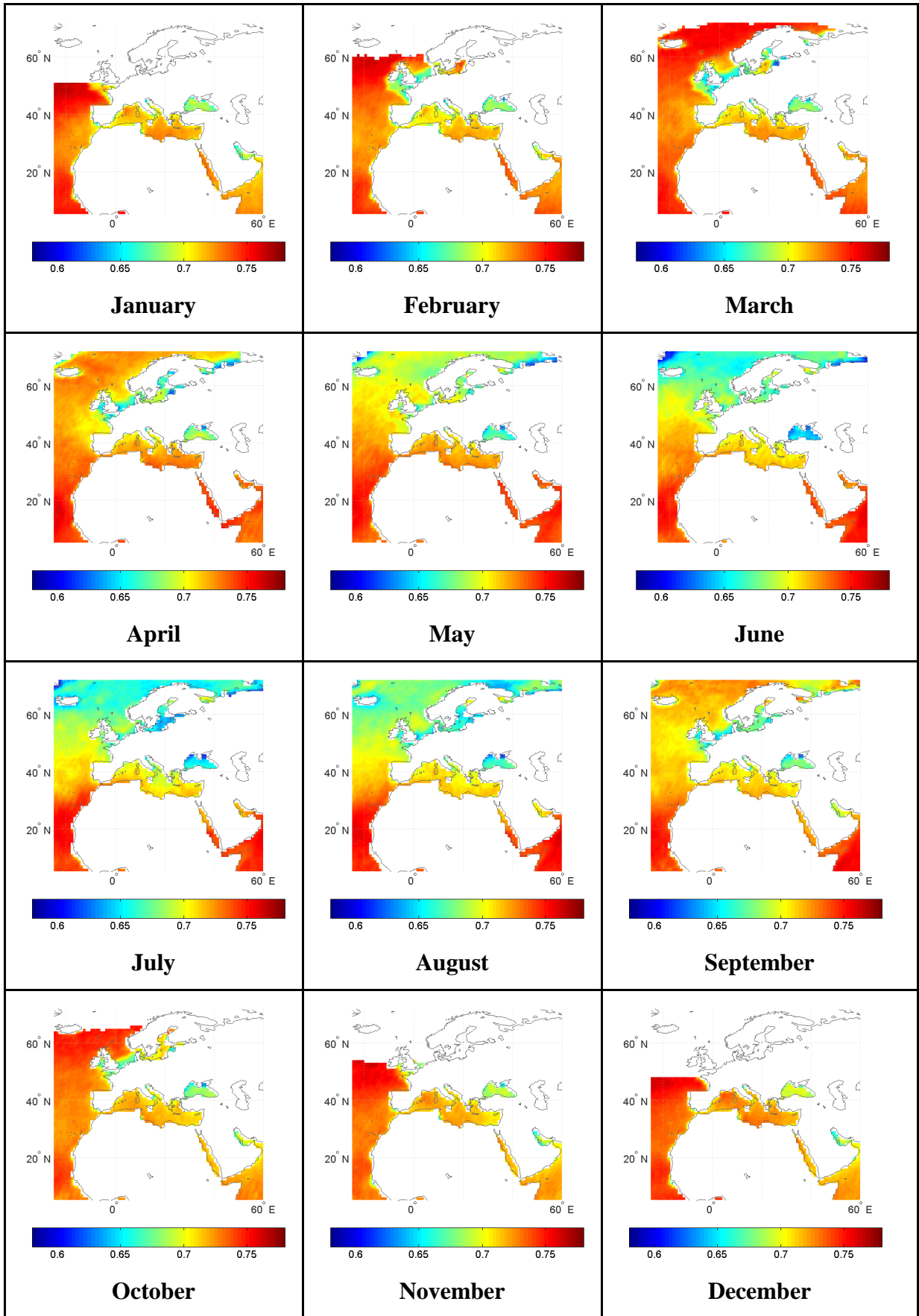
1060



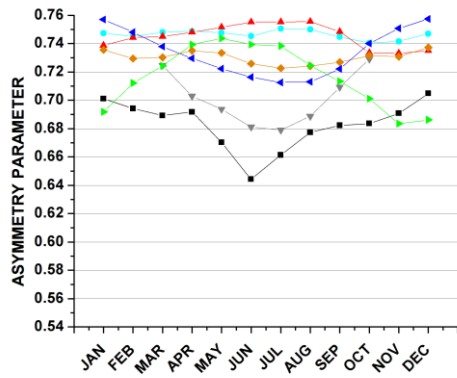
1064

1065 **Figure 2.** Geographical distribution of MODIS-Terra (-a, left column) and MODIS-
 1066 Aqua (-b, right column) g_{aer} values averaged over 2002-2010, at the wavelengths of:
 1067 470 nm (i-, top row), 660 nm (ii-, middle row) and 870 nm (iii-, bottom row).

1068

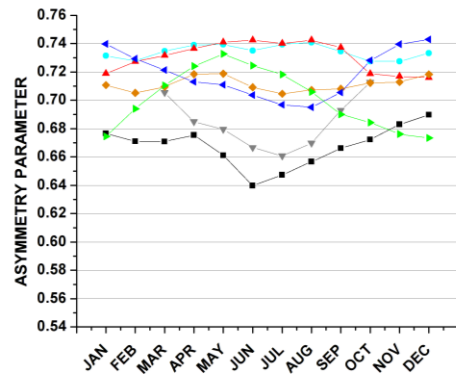


1070 **Figure 3.** Month by month variation of MODIS-Aqua g_{aer} values at 470 nm averaged
1071 over the period 2002-2010.
1072

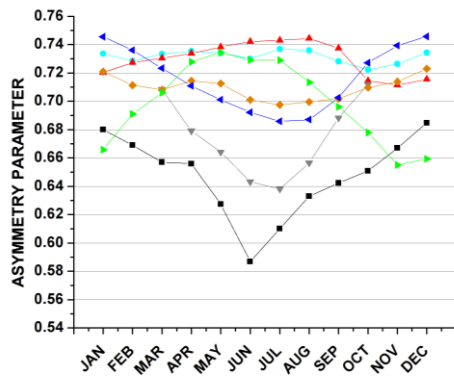


1073

(i-a)

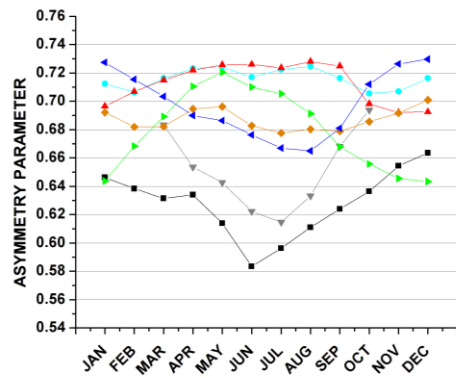


(i-b)

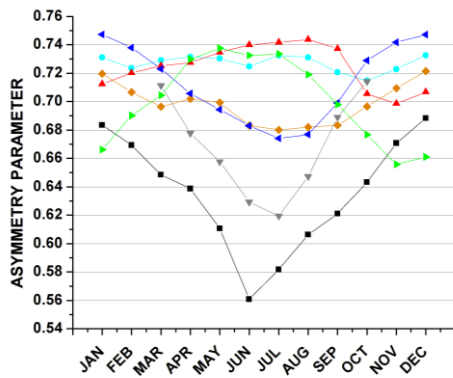


1074

(ii-a)

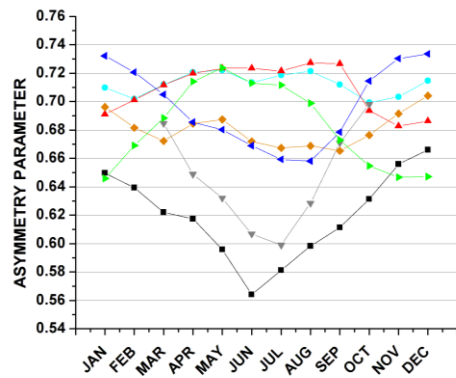


(ii-b)



1075

(iii-a)



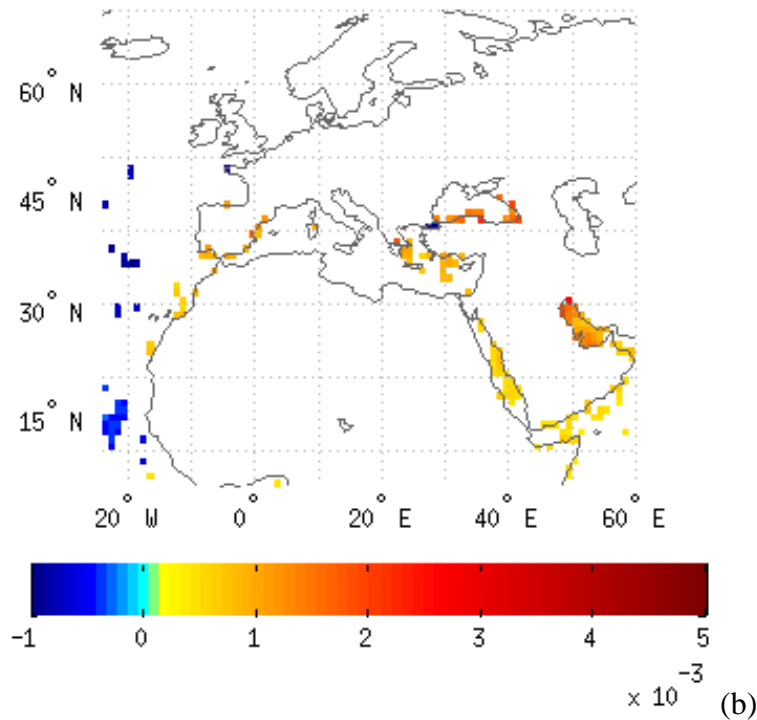
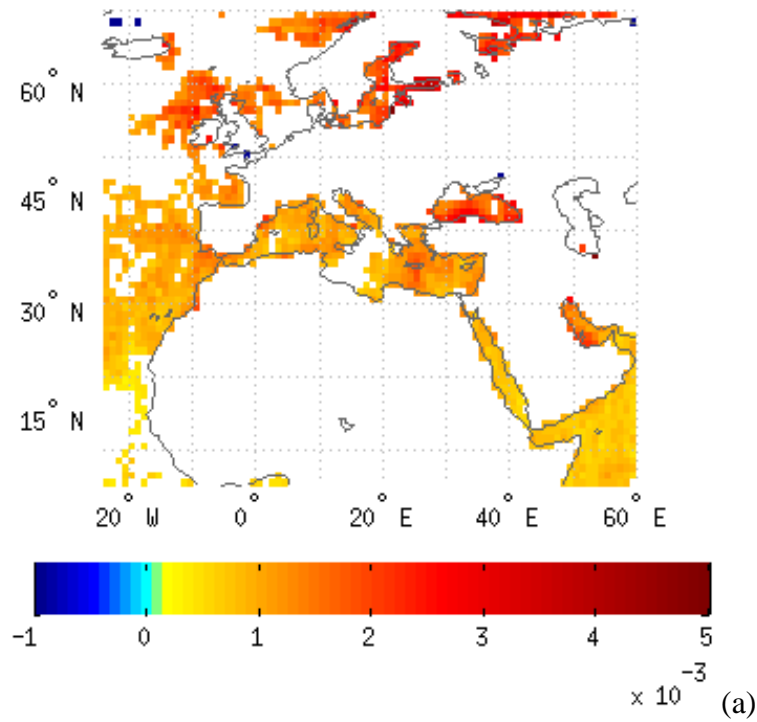
(iii-b)



1076

1077 **Figure 4.** Intra-annual variation of MODIS Terra (-a, left column) and Aqua (-b, right
 1078 column) g_{aer} values averaged over seven selected sub-regions (Fig. 1). Results are
 1079 given for g_{aer} values at: 470 nm (i-, top row), 660 nm (ii-, middle row) and 870 nm
 1080 (iii-, bottom row), averaged over the period 2002-2010, respectively.

1081

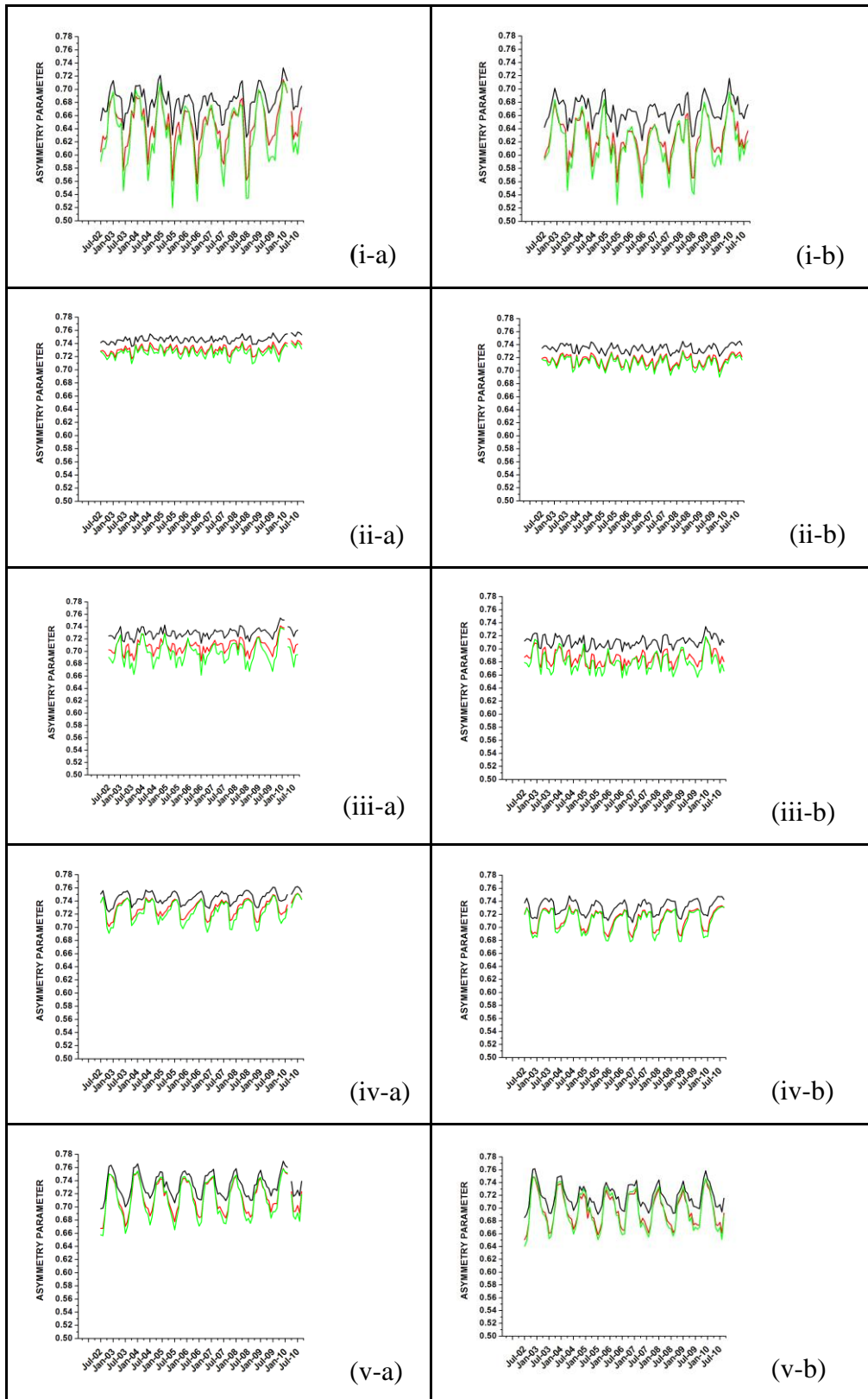


1083

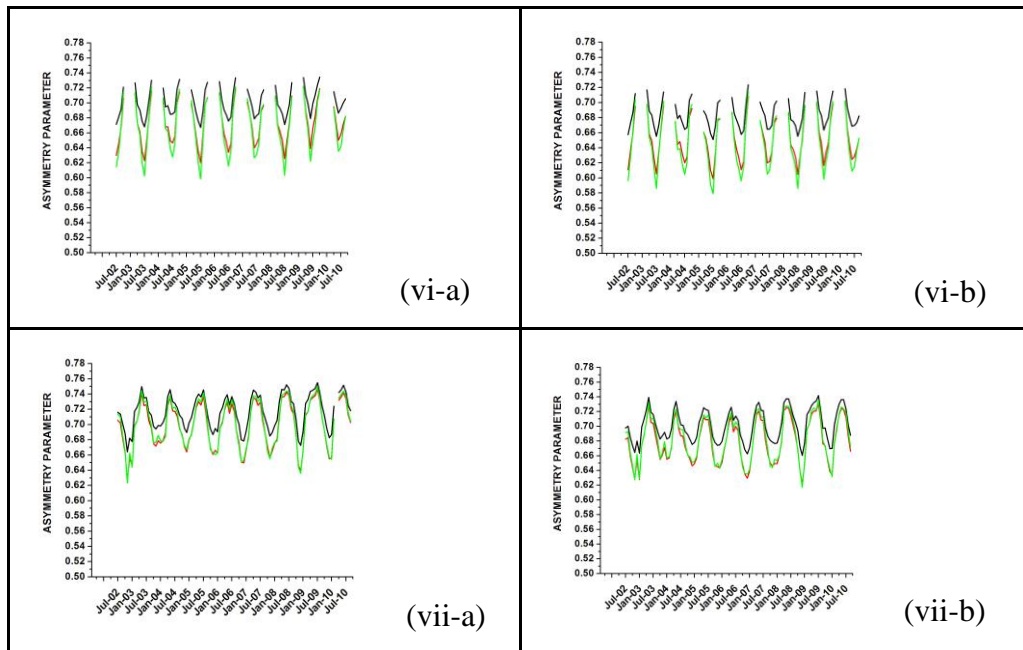
1084

1085 **Figure 5.** Slope (in units decade⁻¹) of MODIS g_{aer} deseasonalized anomalies over the
 1086 period 2002-2010 from MODIS-Terra (-a, top) and MODIS-Aqua (-b, bottom), for
 1087 the wavelengths of 470 nm. Results are shown only if the trend is statistically
 1088 significant at the 95% confidence level.

1089



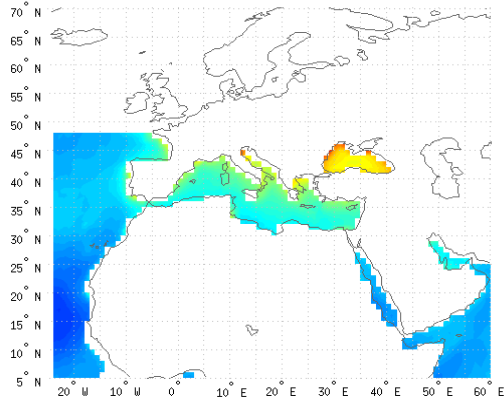
1093 **Figure 6.** Inter-annual (2002-2010) variation of monthly mean g_{aer} values at 470 nm
1094 averaged over the sub-regions of: (i) Black Sea, (ii) Eastern Atlantic Ocean, (iii)
1095 Mediterranean Sea, (iv) Middle East, (v) North-eastern Atlantic Ocean, (vi) North
1096 Europe and (vii) Persian Gulf. Results are given based on MODIS-Terra (-a, left
1097 column) and MODIS-Aqua (-b, right column).
1098



1100

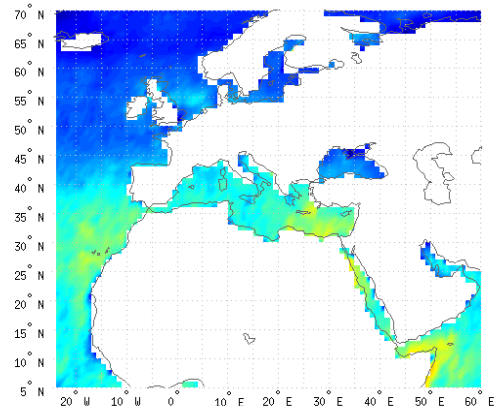
1101 **Figure 6 (continued).** Inter-annual (2002-2010) variation of monthly mean g_{aer} values
 1102 at 470 nm averaged over the sub-regions of: (i) Black Sea, (ii) Eastern Atlantic Ocean,
 1103 (iii) Mediterranean Sea, (iv) Middle East, (v) North-eastern Atlantic Ocean, (vi) North
 1104 Europe and (vii) Persian Gulf. Results are given based on MODIS-Terra (-a, left
 1105 column) and MODIS-Aqua (-b, right column).

1106



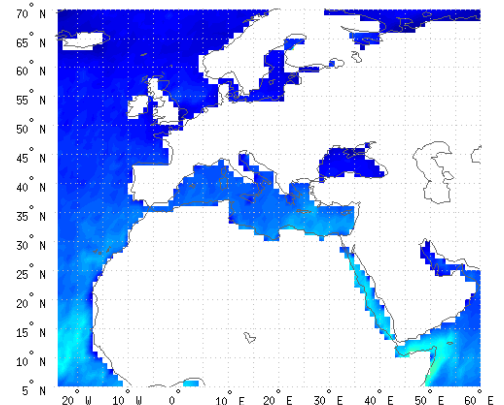
1107

(a)



1108

(b)



1109

(c)

1110

1111

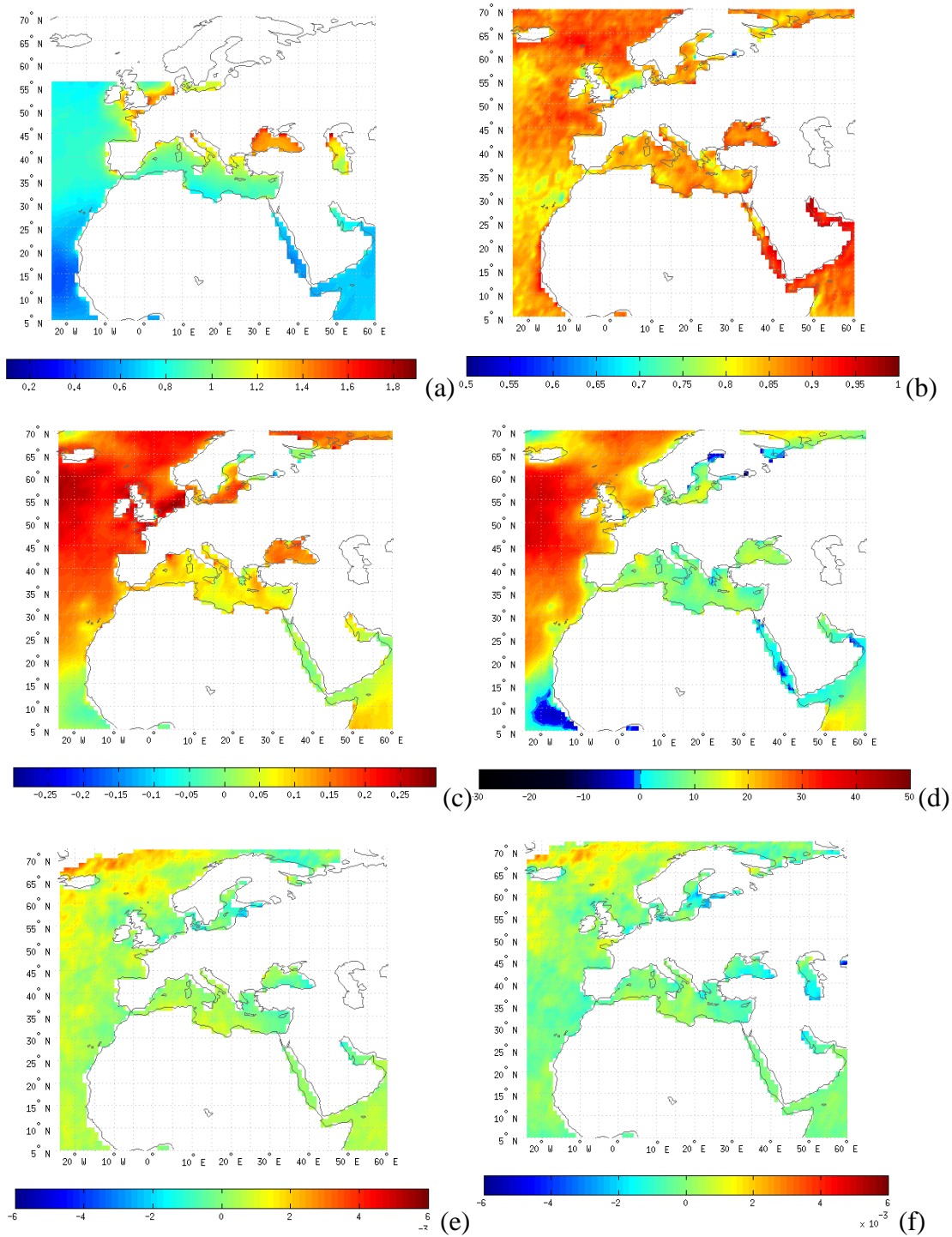
1112

1113

Figure 7. (a) Geographical distribution of MODIS-Aqua \AA Angstrom exponent ($AE_{550-865}$) values averaged over 2002-2010, at the wavelength pair of 550-865nm. Winter AE data are missing from the northernmost areas and therefore the

1114 | long-term averages in (a) are left blank. The correlation coefficients between $AE_{550-865}$
 1115 | and g_{aer} data at 660 and 870 nm are given in (b) and (c), respectively.

1116



1119

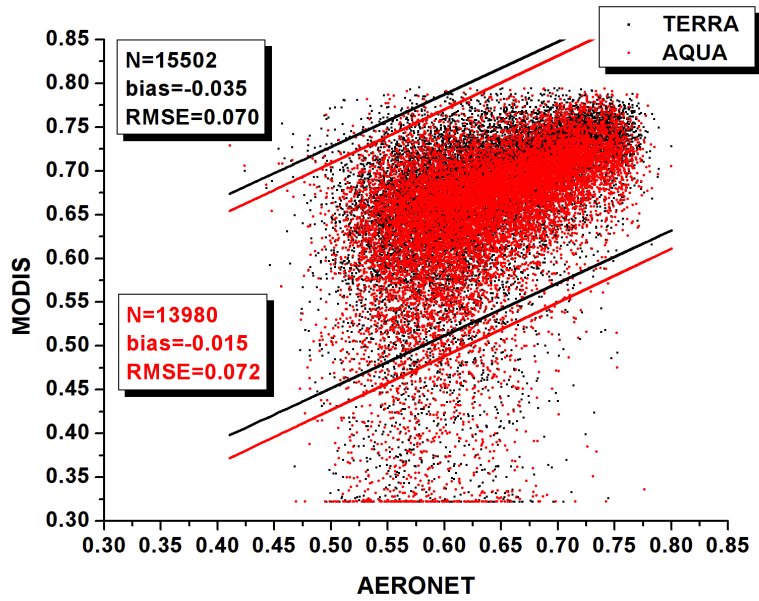
1120

1121 | **Figure 8.** (a) Geographical distribution of MODIS-Aqua C006 Angstrom exponent
 1122 | ($AE_{550-865}$) values averaged over 2002-2010, at the wavelength pair of 550-865nm.

1123 | Winter AE data are missing from the northernmost areas and therefore the long-term
 1124 | averages in (a) are left blank. In (b), (c) and (d) are given the correlation coefficients,

1125 the absolute biases and the relative percent biases, respectively, between the C006 and
1126 corresponding ~~051C005~~ AE₅₅₀₋₈₆₅ data. In (e) and (f) are given the computed
1127 deseasonalized trends of MODIS Aqua ~~051C005~~ and C006 AE₅₅₀₋₈₆₅) slope values for
1128 years 2002-2010, respectively.

1129



1130

1131

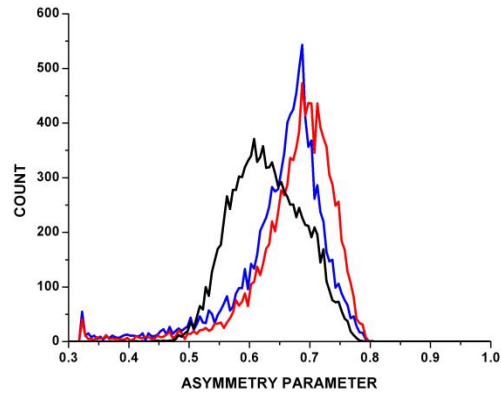
1132 **Figure 9.** Scatterplot comparison between g_{aer} values at 870 nm from MODIS Terra

1133 (black color) and Aqua (red color) and corresponding values from AERONET stations

1134 (blue squares, Fig. 1). The 95% prediction bands as well as the mean bias (AERONET

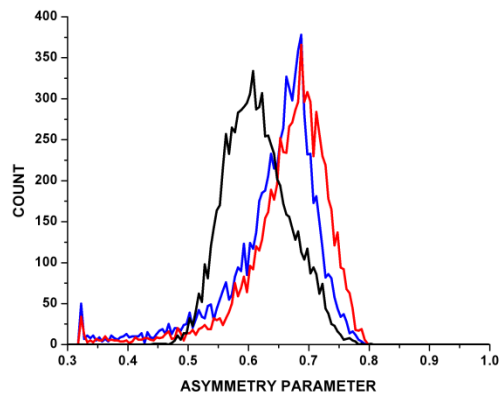
1135 minus MODIS) and root mean squared error are given.

1136



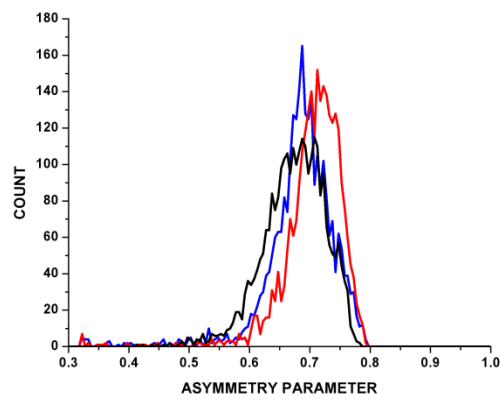
(a)

1137



(b)

1138



(c)

1139

1140

1141

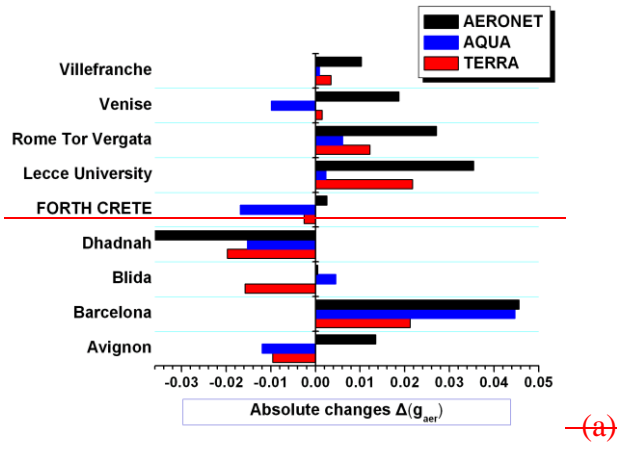
1142

1143

1144

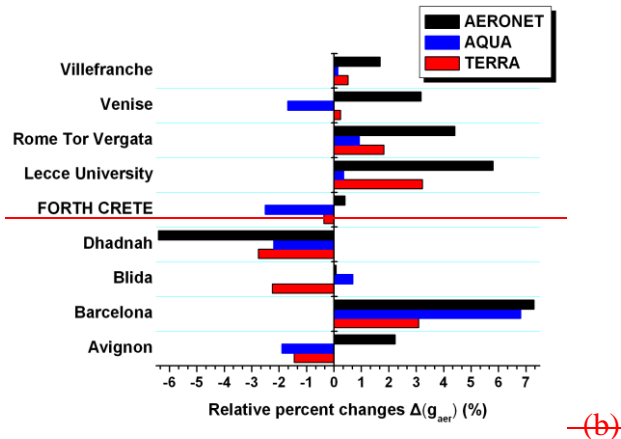
Figure 10. Frequency distribution histograms for MODIS-Terra (red colored lines) MODIS-Aqua (blue-colored lines) and AERONET (black lines) g_{aer} values at 870 nm. The histograms are given separately for: (a) the entire study region, (b) Europe and (c) Africa, Middle East and Arabian peninsula.

1145



(a)

1146



(b)

1147

1148

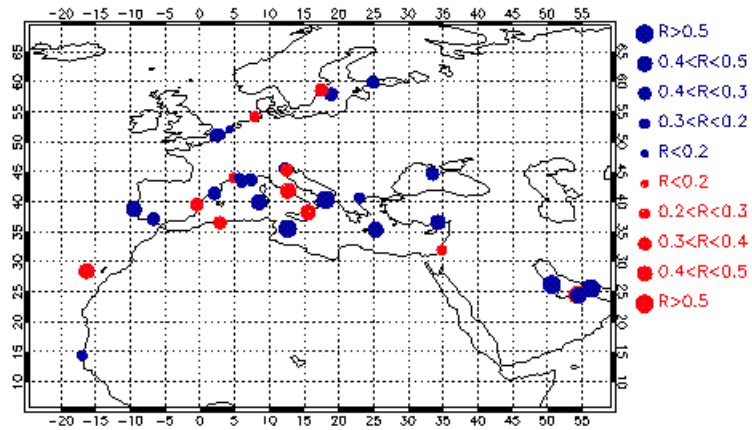
1149

1150

1151

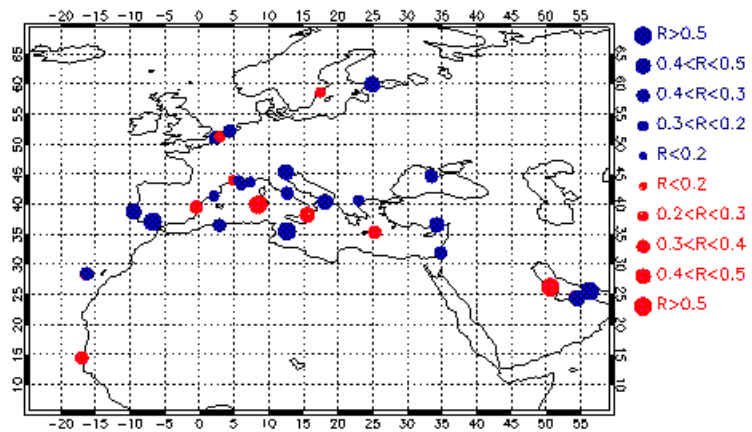
Figure 11. Frequency distribution histograms for MODIS-Terra (red colored lines) MODIS-Aqua (blue colored lines) and AERONET (black lines) g_{aer} values at 870 nm. The histograms are given separately for: (a) the entire study region, (b) Europe and (c) Africa, Middle East and Arabian peninsula.

1152



(a)

1153



(b)

1154

1155

Figure 1211. Map distribution of correlation coefficients between: (i) MODIS-Terra and AERONET g_{aer}

1156

values at 870 nm (left column) and (ii) MODIS-Aqua and AERONET g_{aer} values at 870 nm (right column).

1157

The size of circles corresponds to the magnitude of correlation coefficients, while blue and red colors are

1158

used for stations for which MODIS and AERONET indicate same and opposite tendency of g_{aer} ,

1159

respectively.

1160

1161